

Modeling Soluble Gas Exchange in the Airways and Alveoli

JOSEPH C. ANDERSON,¹ ALBERT L. BABB,¹ and MICHAEL P. HLASTALA^{2,3}

¹Department of Chemical Engineering, ²Department of Medicine, and ³Department of Physiology and Biophysics,
University of Washington, Seattle, WA

(Received 25 April 2003; accepted 16 September 2003)

Abstract—A mathematical model of heat, water and soluble gas exchange in the airways and alveoli was used to predict the location of soluble gas exchange in the lung. A previously published model of heat, water and soluble gas exchange in the *airways* was improved by incorporating anatomical data on the airway wall to better describe the bronchial circulation and expanding the model to include a time varying description of soluble gas concentration in the alveoli. Next, the model was validated using two experimental data sets from the literature: (1) ethanol expirograms and (2) the uptake of seven soluble gases. Then, the model simulated the excretion of ten soluble gases whose blood:air partition coefficient ($\lambda_{b:a}$), a measure of blood solubility, ranged over 5 orders of magnitude. We found that gases with $\lambda_{b:a} < 10$ exchange almost solely in the alveoli and gases with $\lambda_{b:a} > 100$ exchange almost exclusively in the airways. Gases with $\lambda_{b:a}$ between 10 and 100 have significant interaction with the airways and alveoli. These results suggest that the airways play a larger role in pulmonary gas exchange than previously assumed and may require a reevaluation of pulmonary tests that involve exhaled samples of gases with $\lambda_{b:a} > 10$. © 2003 Biomedical Engineering Society.
[DOI: 10.1114/1.1630600]

Keywords—Mathematical model, Bronchial circulation, Inert gas.

INTRODUCTION

Over the past five decades, the major focus of pulmonary gas exchange research has rightly been on gas exchange in the alveoli. From the simple gas exchange model developed by Farhi¹⁰ that described the lungs as one large alveolar unit to the more complex multiple inert gas elimination technique proposed by Wagner *et al.*⁴⁶ that helped to quantify gas exchange heterogeneity among alveolar units, the models of alveolar gas exchange were developed and refined because the gases most important to life, O₂ and CO₂, exchange there. From this multitude of studies, respiratory physiologists learned that alveolar gas exchange is dependent on ventilation, pulmonary perfusion, and the blood:air partition

coefficient, $\lambda_{b:a}$. Of these three parameters, the blood:air partition coefficient, $\lambda_{b:a}$, is arguably the most important because it determines that low blood-soluble gases ($\lambda_{b:a} < 10$) must exchange in the alveoli.

Over the past thirty years, some pulmonary physiologists have also been investigating another avenue of pulmonary gas exchange—the airways. However, the gases that exchange in the airways are not respiratory gases but solvent gases that are very water soluble and have a high blood solubility ($\lambda_{b:a} > 1000$). In this laboratory, a mathematical model describing the exchange of water, heat, and a soluble gas in the upper airways was developed⁴² and fitted with experimental temperature profiles⁴² and ethanol data.¹³ Using this model, our laboratory has determined that gas exchange in the airways is similar to alveolar gas exchange in that gas exchange in both regions are highly dependent on ventilation and $\lambda_{b:a}$. However, unlike alveolar gas exchange, diffusion of gas through the airway tissue and bronchial blood flow are also important factors determining airway gas exchange.

While the exchange mechanisms for gases at each end of the blood solubility spectrum have been closely examined, the location and the exchange mechanisms of gases residing between these two extremes ($10 < \lambda_{b:a} < 1000$) has not been quantified. In this study, we took our previously published model of heat, water, and soluble gas exchange in the *airways* and improved the description of the bronchial circulation by incorporating anatomical data on the bronchial circulation and airway wall. Then, the model was expanded to include a time varying description of soluble gas concentration in the alveoli and to allow soluble gas to enter the lungs from either or both the inspired air or/and circulating blood. To provide accurate predictions of pulmonary gas exchange, the mathematical model was validated using two sets of experimental data. The first validation used exhaled ethanol profiles measured by George *et al.*¹³ The model was matched to these data by adjusting bronchial blood flow, \dot{Q}_{br} . The second validation used data from a short 10 min washin of seven soluble gases with blood:air partition coefficient ranging from 90 to

Address correspondence to Michael P. Hlastala, Ph.D., Division of Pulmonary and Critical Care Medicine, Box 356522, University of Washington, Seattle, WA 98195-6522. Electronic mail: hlastala@u.washington.edu

12 000.²⁹ Matching the model with the end-expired and mixed-expired data from that experiment was also accomplished by adjusting \dot{Q}_{br} . Then, the validated pulmonary (airway and alveolar) model of gas exchange was used to predict the exchange of ten soluble gases ($0.09 < \lambda_{b:a} < 2709$) and thereby address the primary question of this study. How does the blood:air partition coefficient affect the location of soluble gas exchange in the lung?

It was hypothesized that the location and extent of soluble gas exchange in the lungs was highly dependent on the blood:air partition coefficient. Gases with a low blood:air partition coefficient exchange completely in the alveoli while high blood-soluble gases exchange completely in the airways. Intermediate blood-soluble gases exchange partially with the airways and the alveoli.

MATHEMATICAL MODEL

The original mathematical model described the simultaneous exchange of heat, water, and a soluble gas with the airways. The initial detailed model derivation and validation with airway temperature profiles was published by Tsu *et al.*⁴² Validation with exhaled ethanol profiles and further model modifications were published by George *et al.*¹³ The current model, described here, now includes the bronchial circulation, pulmonary circulation and a time-dependent alveolar compartment. All of these modifications are presented here with a brief description of the airway wall parameters (including bronchial circulation) and model equations (Appendix).

Axial Structure. The lung model has a symmetrically bifurcating structure through eighteen Weibel generations. The dimensions (lengths and diameters) for the upper respiratory tract (nasal and oral) are taken from Hanna and Scherer.¹⁶ The lower respiratory tract dimensions are taken from Weibel.⁴⁷ Because the dimensions of Weibel's model were determined at a volume of three-fourths total lung capacity (4800 ml), these dimensions were scaled. For model simulations involving tidal breathing, the airway lengths and diameters were scaled by a factor $(2650/4800)^{1/3}$ to represent a functional residual capacity (FRC) of 2650 ml.²¹ When the model simulated a single exhalation maneuver, an exhalation from TLC to RV, the lung was not scaled (i.e., airway dimensions = $\frac{3}{4}$ TLC). The airway dimensions for tidal breathing or a single exhalation maneuver were scaled to account for the size of the subject. Since the vital capacity of the Weibel lung model is ~ 5000 ml, the dimensions were scaled by a factor $(VC/5000)^{1/3}$ where VC is vital capacity. Axially, the model is divided into 480 control volumes (discussed in the following section)

from the mouth to the 18th generation. The alveoli and respiratory bronchioles are lumped into a single alveolar unit (i.e., 481st control volume).

Previous versions of this model^{13,42} only allowed soluble gas to enter the lung from the bronchial and pulmonary circulations and assumed the alveolar air to always be fully saturated with water and soluble gas at body temperature (37 °C). These two restrictions were relaxed in this model version. First, the current model allows soluble gas to enter the lung from the inspired air, from the circulating blood or from both the air and blood. Second, the mole fraction of soluble gas in the alveolar air is allowed to vary with time as described by a mass balance on the alveolar compartment (see Appendix for a brief description). This time-dependent alveolar compartment will not affect the exchange of high blood-soluble gases such as ethanol ($\lambda_{b:a} = 1756$) but this compartment will be important when simulating the exchange of gases with $\lambda_{b:a} < 100$. Pulmonary blood flow, \dot{Q}_p , is assumed to be 100 ml s^{-1} which approximately matches the ventilation rate for the studies modeled here. The pulmonary blood volume, V_p , is assumed to be 100 ml resulting in a pulmonary capillary residence time of 1 s.² The alveolar volume, V_A , at FRC was assumed to be 2650 ml which is characteristic of a FRC of a healthy young man.²¹

Since the mole fraction of soluble gas in the alveolar compartment can vary with time, the mole fraction of soluble gas in the pulmonary artery is not necessarily equal to the mole fraction of soluble gas in the bronchial artery. In the current model, the soluble gas mole fraction in the bronchial artery, X_a , is assumed to be equal to the soluble gas mole fraction leaving the pulmonary circulation. This assumption will not affect the exchange of high blood-soluble gases such as ethanol but it will be necessary when simulating the exchange of gases with $\lambda_{b:a} < 100$.

Radial Structure: General. In earlier models,^{13,42} the radial structure of the airway control volume consisted of four compartments: (1) the airway lumen; (2) a thin layer of mucus; (3) a nonperfused tissue layer that represents the respiratory epithelium, basement membrane, and any connective tissue before reaching (4) the capillary bed of the bronchial circulation. This capillary bed was considered to be an infinite source or sink for heat and the soluble gas; that is, the temperature and mole fraction of the soluble gas in the bronchial circulation were constant. In a recent version of this model,⁶ the structure of this capillary bed was modified to allow the temperature and soluble gas mole fraction to vary with time and axial position. Thus, the effects of airway perfusion on airway gas exchange could be studied.

In this current model (Fig. 1), the airways are divided into six radial compartments: (1) the airway lumen, (2) a

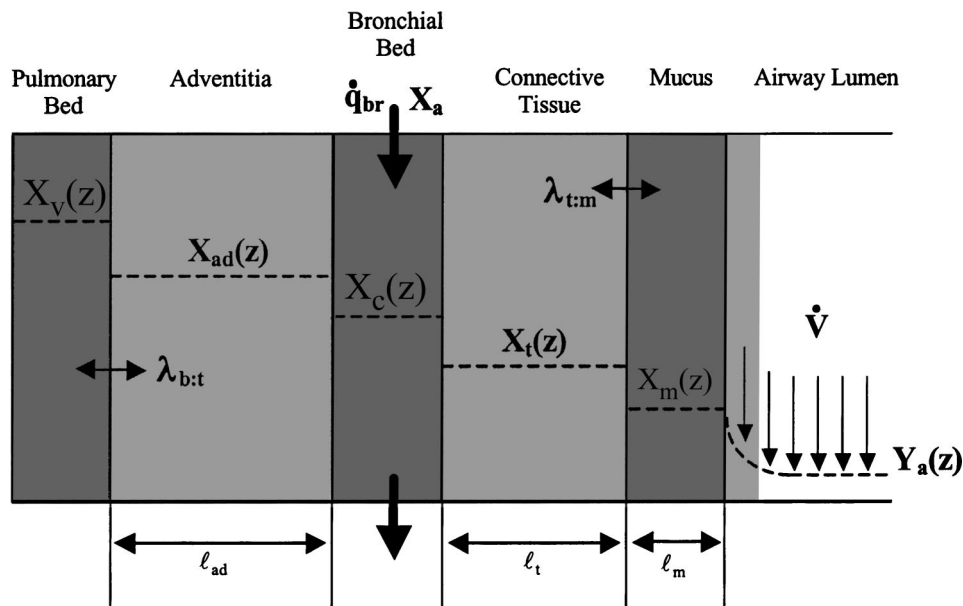


FIGURE 1. Model control volume. The source of soluble gas for this diagram is the blood (pulmonary venous and bronchial arterial). Blood enters the bronchial bed compartment with mole fraction, X_a . Soluble gas is transported by secretion and diffusion across a series of annular layers before entering the passing airstream. The ratio of gas solubility between layers is specified by a partition coefficient, λ . The shaded region in the airway lumen represents the boundary layer resistance associated with the air–mucus interface. The thickness of the connective tissue compartment, ℓ_t , and the thickness of the adventitial layer, ℓ_{ad} , represent recently measured parameters that characterize the newly incorporated bronchial circulation and adventitial layers.

thin mucous layer, (3) a connective tissue layer, (4) the bronchial circulation, (5) the adventitial layer, and (6) the pulmonary circulation. Within a control volume, the surface area for exchange between radial layers, A_s , is assumed to be constant and equal to $\pi d \Delta z$ where d is the diameter of the airway lumen and Δz is the axial length of the control volume. The soluble gas mole fraction, water content, and temperature are assumed to be uniform within each radial layer. Gas transfer between layers occurs by radial diffusion and secretion. Axial diffusion of energy and mass between similar layers of adjacent control volumes is neglected except for mass in the airway lumen. A brief derivation of the energy and mass balances for each layer is in the Appendix.

Airway Lumen. Within this layer, the air consists of a tertiary system of soluble gas, water and dry air. Mass and energy are transported between control volumes by bulk convection and axial diffusion for mass as described by Tvedt.⁴⁴ The diffusivity of soluble gas through air was calculated using the Wilke–Lee modification of the Hirschfelder–Bird–Spotz method.⁴¹ Between the air and mucus, the heat transfer coefficient is described by an empirical correlation derived by Ingenito²² and the mass transfer coefficient is calculated from the Chilton–Colburn analogy.⁷ Near the air–mucus interface, local vapor–liquid equilibrium is assumed. This equilibrium is described by Raoult’s law for water and the water:air

partition coefficient, $\lambda_{w:a}$, for the soluble gas. The exchange of O_2 and CO_2 is assumed to have a negligible effect on the soluble gas mole fraction.

Mucus. The mucous layer surrounds the airway lumen and is treated as a binary mixture of water and dilute soluble gas. Because the mucus is $\sim 95\%$ water,³¹ the physical properties of the mucus are assumed to be equal to those found in water. The mucous layer thickness varies with local hydration and dehydration. A minimum thickness ($10 \mu\text{m}$ in the trachea) is maintained by secretions from the bronchial bed. A minimum thickness is maintained in each generation such that the volume of mucus across a generation is equal to the minimum volume in the trachea.

Connective Tissue. The tissue layer is treated as a binary mixture of dilute soluble gas and water (i.e., the physical properties of tissue are assumed to be equivalent to water). The diffusivity of soluble gas through the connective tissue is assumed to be 33% of its diffusivity in water.¹² The diffusivity of soluble gas through water was calculated using the Wilke–Chang method.⁵⁰ The solubility of gas in tissue is described by two partition coefficients. For most gases, the blood:tissue partition coefficient, $\lambda_{b:t}$, is assumed to equal one but for ethane, cyclopropane, halothane, ether, and acetone, $\lambda_{b:t}$ is equal to 1.18, 1.63, 1.27, 1.53, and 1.38, respectively.⁵³ The

tissue:mucus partition coefficient, $\lambda_{t:m}$, is calculated by relating the partition coefficient between radial layers to one another:⁴⁴

$$\lambda_{t:m}(T) = \frac{1}{\lambda_{b:t}(T)} \left(\frac{\lambda_{b:a}(T)}{\lambda_{m:a}(T)} \right). \quad (1)$$

The mucus:air partition coefficient is assumed to be equal to the water:air partition coefficient ($\lambda_{m:a} = \lambda_{w:a}$). To maintain a constant tissue volume, fluid is filtered from the bronchial bed to replace the fluid that was lost maintaining a minimum mucous thickness. The thickness of this layer for each airway generation was determined from bronchial vessel measurements in sheep³ that were scaled to humans (see below in Model Dimensions for Airway Wall).

Bronchial Capillary Bed. In the earliest versions of this model,^{13,43} the bronchial bed was described as an infinite source for heat and mass implying airway gas exchange to be dominated by diffusion through the connective tissue. However, more recent experimental^{39,40} and theoretical investigations^{6,14} demonstrated that airway gas exchange depends strongly on the tissue diffusing capacity and perfusion of the airway wall. Thus, the current model reflects these dependencies through the development of a bronchial bed layer that uses new measurements of the bronchial circulation.³

The bronchial bed is modeled as an axial series of annular sheets of blood that surround the tissue layer. The blood entering each control volume has a soluble gas mole fraction, X_a , and a temperature, T_b , equal to body temperature (37°C). Within each control volume, blood exchanges heat and mass with the tissue layers, fluid is filtered from the capillary bed to the connective tissue layer exactly replacing the fluid lost from the tissue by secretion, and the blood exits the bronchial bed with a soluble gas mole fraction, X_c , and temperature, T_c . The blood is considered well mixed both axially and radially. Each control volume contains an individual vessel that is characterized by three parameters.

The first parameter is the total blood flow rate to the airways, \dot{Q}_{br} (ml s⁻¹), and is defined as the sum of all of the control volume blood flow rates:

$$\dot{Q}_{br} = \sum_{n=1}^I \dot{q}_{br}(z), \quad (2)$$

where I is the total number of control volumes and is defined to be

$$I = \sum_{n=1}^N i(n) 2^{g(n)}, \quad (3)$$

where N is the total number of compartments in the model, $i(n)$ is the number of control volumes in compartment n , and $g(n)$ is the airway generation number. Although total blood flow can be specified, local blood flow to a control volume at axial position z is calculated using the following relationship:

$$\dot{q}_{br}(z) = v_t(z) \bar{q}_{br} F(z). \quad (4)$$

The variable $v_t(z)$ is the volume of tissue (cm³) surrounding the airway at axial position z , \bar{q}_{br} is the mean blood flow per unit volume of tissue, and $F(z)$ is a weighting factor given by Bernard *et al.*⁵ These parameters are defined by the following relationships:

$$F(z) = 0.19 + 2.8 \exp[-5.1d(z)], \quad (5)$$

$$\bar{q}_{br} = \frac{\dot{Q}_{br}}{V_t}, \quad (6)$$

$$V_t = \sum_{n=1}^I v_t(z). \quad (7)$$

The second and third parameters are the bronchial capillary surface area and capillary volume, respectively. These two parameters and the connective tissue thickness, ℓ_t , were recently measured in sheep.³ These three parameters provide a stronger quantification of bronchial capillary diffusing capacity and residence time than previous models of airway gas exchange.

Adventitial Tissue. The adventitial layer resides between the bronchial bed and the pulmonary bed where the pulmonary capillary conditions are assumed to exist. The physical properties of this layer are assumed to be equivalent to water with the exception of solubility and diffusivity (see above in Connective Tissue). The thickness of this layer was calculated by subtracting the connective tissue thickness (see below in Model Dimensions for Airway Wall) from the lumen-alveolar tissue thickness. The lumen-alveolar tissue thickness was calculated as the sum of the airway wall tissue thickness and the epithelial thickness (Table 1). In the current model, this layer is present for generations three and greater, the intraparenchymal airways. For airway generations three through ten, cartilage resides in the adventitial tissue and is thought to impede the diffusion of soluble gas through this tissue.¹⁵ As a result, the molecular diffusivity of soluble gas through this layer was assumed to be 10% of the molecular diffusivity through the connective tissue (i.e., ~3% of the molecular diffusion coefficient of soluble gas through water).

TABLE 1. Bronchial vasculature measurements and airway wall measurements from sheep and humans used to estimate the airway wall and bronchial bed dimensions.

Analysis	Best fit line	Reference
Sheep measurements		
Epithelial thickness	$y=0.00148d+0.0022$	3
Connective tissue thickness	$y=0.0012d+0.004$	3
Wall tissue thickness	$y=0.0847d+0.0056$	3
$\sqrt{\text{Capillary cross-sectional area}}$	$y=0.0118d+0.003$	3
$\sqrt{\text{Wall area}}$	$y=0.554d$	3
Human measurements		
Epithelial thickness	$y=0.0052d+0.0016$	11
$\sqrt{\text{Wall area}}$	$y=0.306d+0.014$	30

All variable dimensions are in centimeters. The variable d is the airway diameter.

Pulmonary Capillary Bed. The pulmonary bed layer is assumed to be an infinite source or sink of heat and mass. The temperature is assumed to be constant at a body temperature of 37 °C. The mole fraction of soluble gas in this layer, X_{pb} , is assumed to be the average of the soluble gas mole fraction entering the pulmonary circulation, X_v , and bronchial circulation, X_a (i.e., leaving the pulmonary circulation). For extremely blood-soluble gases like ethanol, $X_{pb} \approx X_v$. For a soluble gas very much less soluble than ethanol (e.g., ether), $X_a < X_{pb} < X_v$. In the current model, this layer is present for airway generations three and greater, namely, the intraparenchymal airways.

Boundary Conditions. Boundary conditions are applied at the mouth and alveoli. During inspiration, the ambient temperature and relative humidity of the inspired air are set equal to 23 °C and 50%, respectively. The mole fraction of soluble gas in the inspirate can be set equal to zero to study the elimination of soluble gas from the body or to a finite value to study the uptake of soluble gas from the ambient air. For all times, the alveolar air is assumed to be fully saturated with water and to have a temperature equal to a mean body core temperature of 37 °C. The mole fraction of soluble gas in the alveolar compartment varies with time based on a mass balance. In the respiratory tract, local vapor–liquid equilibrium is assumed at the air–mucus interface. This equilibrium is described by Raoult’s law for water and by the mucus:air partition coefficient, $\lambda_{m:a}$, for soluble gas. Between radial layers, partition coefficients are used to define the solubility of gas in one layer relative to another.

Solution of Model Equations

Mass and energy balances around each control volume produce twelve differential equations in time, t , and space, z . The equations are solved simultaneously for the following twelve dependent variables: the mole fraction

of soluble gas in the air, mucous, connective tissue, bronchial bed, and adventitial tissue layers ($Y_a, X_m, X_t, X_c, X_{ad}$); the temperature of the air, mucous, connective tissue, bronchial bed, and adventitial tissue layers ($T_a, T_m, T_t, T_c, T_{ad}$); the mole fraction of water in the air (Y_w); and the mucous thickness (ℓ_m). The twelve differential equations are solved numerically on a Pentium IV computer running DIGITAL VISUAL FORTRAN. The spatial dimensions are solved by upstream finite difference while the time derivatives are handled using LSODE, an integrating software package developed by Hindmarsh.¹⁸ The mass balance around the alveolar compartment is integrated separately from the airway control volumes using LSODE. On inspiration, the mole fraction and temperature of gas leaving the last control volume in generation 18 become the input conditions for the alveolar compartment. On exhalation, the mole fraction and temperature of gas leaving the alveolar compartment become the input conditions for generation 18.

Simulating Steady-State Gas Exchange

Before the model simulates any tidal or prolonged breathing maneuvers, the model first must reach breath-to-breath steady-state conditions. In general, the temperature, water concentrations, and soluble gas concentrations within the mathematical model were brought to steady state by simulating 30 tidal breaths from FRC.⁴³ A respiratory rate of 12 breaths/min, a sinusoidal flow waveform, a tidal volume of 500 ml, and a vital capacity of 5000 ml were used. Additionally, the inspired air temperature and relative humidity was set at 23 °C and 50%, respectively. Depending on the simulation, soluble gas enters the lung from either the inspired air or the pulmonary circulation.

Model Dimensions for Airway Wall

A major improvement to the current airway gas exchange model is the use of anatomical measurements of

the bronchial circulation and thickness of airway tissue. Four measurements, made in sheep,³ provide a means to accurately describe the dependence of airway gas exchange to diffusion through the airway tissue and perfusion of the airways via the bronchial circulation. Two of these measurements, the capillary perimeter (i.e., surface area) and the connective tissue thickness, completely specify the diffusing capacity of the bronchial circulation. The diffusion coefficient of heat and mass in tissue and the tissue solubility of a soluble gas are reasonably well known. The third measurement, capillary volume, can be calculated from the capillary cross-sectional area and provides a description of the perfusion dependence of airway gas exchange on the bronchial circulation. The fourth measurement, the wall tissue thickness, is the distance between the airway lumen and the alveolar-adventitial boundary. Subtraction of the connective tissue thickness from the wall tissue thickness provides a measure of the adventitial layer thickness.

The measurements of tissue thickness and capillary cross-sectional area were scaled to humans using the following method. Each sheep parameter was normalized by a second sheep tissue measurement. This second measurement had two characteristics: (1) a similar functionality with airway diameter as the first and (2) a corresponding measurement in humans. For example, the connective tissue thickness was normalized by epithelial thickness in sheep (Table 1), and the capillary cross-sectional area was normalized by the airway wall area in sheep (Table 1). To determine the connective tissue thickness and capillary cross-sectional area in humans, the normalized measurements were multiplied by the epithelial thickness in humans and the airway wall area in humans, respectively (Table 1). The bronchial capillary volume, v_c , was calculated by multiplying the bronchial capillary cross-sectional area by the thickness of the control volume, Δz . The bronchial capillary perimeter (i.e., surface area) was also measured in sheep but was not scaled for humans as it was found to equal 58% of the airway lumen surface area for all airway generations. The capillary area fraction is equal to half of the ratio of capillary-to-lumen surface area, $\Phi_c = 0.29$, as half the surface is available for exchange with the airway lumen and the other half with the pulmonary capillary.

Gas Flow From Airway Wall to Lumen

When a subject with soluble gas in their blood breathes fresh air, soluble gas will be absorbed from the

mucus during inspiration and desorbed back to the mucus during expiration. During inspiration each airway generation will contribute a small quantity of soluble gas from the airway wall to the gas stream. The reverse occurs during expiration. Per airway generation or model compartment, the molar flow of soluble gas can be mathematically described by the following expressions for inspiration, j_{insp} , and expiration, j_{exp} :

$$j_{\text{insp}}(n) = 2^{g(n)} \sum_{x=1}^i \left[A_s(x) \left(\frac{k_{y,a}(x)}{\dot{V}_{\text{insp}}(x)} \right) \times \int_{V_{ee}}^{V_{ei}} [Y_a(x,v) - Y_{\text{wall},a}(x,v)] dv \right], \quad (8)$$

$$j_{\text{exp}}(n) = 2^{g(n)} \sum_{x=1}^i \left[A_s(x) \left(\frac{k_{y,a}(x)}{\dot{V}_{\text{exp}}(x)} \right) \times \int_{V_{ei}}^{V_{ee}} [Y_a(x,v) - Y_{\text{wall},a}(x,v)] dv \right], \quad (9)$$

where g is the generation number, i is the number of control volumes in the compartment, x is the control volume number, $k_{y,a}$ is the local mass transfer coefficient for the soluble gas, \dot{V}_{insp} is the volumetric flow rate of air during inspiration, \dot{V}_{exp} is the volumetric flow rate of air during expiration, V_{ee} is the lung volume at end expiration, and V_{ei} is the lung volume at end inspiration. The differential volume, dv , is equal to the differential time element, dt , multiplied by the volumetric flow rate, \dot{V} . Equations (9) and (10) confirm that the main driving force for soluble gas transfer is the difference between the soluble gas mole fraction in the airway lumen, Y_a , and the mole fraction of soluble gas at the air-mucus interface, $Y_{\text{wall},a}$.

Determination of Gas Exchange Location

To determine where the majority of gas exchange occurs (i.e., airway versus alveolar), an exchange ratio (ER) can be defined as the ratio of airway gas exchange to total pulmonary gas exchange [Eq. (10)]:

$$ER = \frac{\text{net airway gas transfer}}{\text{net airway gas transfer} + \text{net alveolar gas transfer}}. \quad (10)$$

As a measure of airway gas exchange, the net mass transfer of inert gas from the airway was calculated as the sum of the inert gas flow from the mucus to the airway lumen on inspiration and the inert gas flow from the mucus to the airway lumen on expiration. For a measure of alveolar gas exchange, the net mass transfer of inert gas from the alveoli was calculated as the sum of the inert gas flow from the alveolar gas to the pulmonary blood on inspiration and the inert gas flow from the alveolar gas to the pulmonary blood on expiration. Total pulmonary gas exchange is defined as the sum of airway net gas transfer and net transfer of inert gas from the alveoli.

MODEL VALIDATION

Ethanol Expirograms

Experimental Single Exhalation Maneuvers. The details of the experimental protocol can be found elsewhere.¹³ The pertinent results are presented here. Six male volunteers ingested enough alcohol to achieve a blood alcohol concentration of approximately 0.09 gm% according to the Widmark formula.⁴⁸ The mean age, weight, and vital capacity for the single-exhalation maneuver were 30 ± 10 yr, 78 ± 14 kg, 5400 ± 740 ml, respectively. Following ingestion of the alcohol, the subjects waited approximately 1 h for absorption to take place. Each subject performed two different breathing maneuvers, repeated five times each. Maneuver A consisted of a single inhalation to total lung capacity (TLC) followed by an exhalation at a slow constant flow rate to residual volume (RV). The second breathing maneuver, maneuver B, was identical to the first except that the exhalation was at a rapid constant flow rate. Ethanol concentration, exhaled volume, and exhaled flow rate were measured dynamically throughout the prolonged exhalation. Quiet tidal breathing was done for three minutes between maneuvers. The expired concentration of ethanol was normalized by the concentration of ethanol in the alveolar gas. Then, each group of expirograms within a subject and maneuver type was condensed into a single representative exhalation maneuver by averaging the normalized alcohol concentration in the exhaled air at intervals of one-tenth the total exhaled volume.

Simulated Single Exhalation Maneuvers. Prior to simulating a breathing maneuver, the airways were brought to steady-state conditions as outlined in the *Simulating Steady-State Gas Exchange* except the tidal volume was approximated to be 10% of the subject's vital capacity¹⁷ and ethanol entered the lung via the pulmonary circulation. To simulate a single exhalation maneuver, the in-

spired volume, expired volume, and exhalation time must be specified. The large inspired volume was approximated to be 65% of each subject's vital capacity.¹⁷ The experimentally measured expired volume for each exhalation maneuver was used in the model. The exhalation time for each maneuver and subject was calculated by dividing the smallest expired volume by the mean flow rate for each group of maneuvers. The single exhalation maneuver was simulated at a lung volume equal to three fourths TLC.

The bronchial blood flow, \dot{Q}_{br} , was used as an adjustable parameter to optimize the fit of the model to the experimental data for each subject and maneuver. The accuracy of the model prediction was evaluated using the method of least squares and summarized with a correlation coefficient (R^2). The best-fit \dot{Q}_{br} was determined to within 0.1 ml s^{-1} .

Short Duration Soluble Gas Washin

Experimental Washin. Detailed results of the experimental protocol have been previously published,²⁹ hence, only the salient results will be presented here. The mean age, weight, height, and tidal volume for the four subjects were 46.5 ± 3.2 (SD) yr, 60.5 ± 13.5 kg, 167.0 ± 8.8 cm, and 500 ± 30 ml, respectively. The mean respiratory rate for inhalation of each soluble gas was $13.0 \pm 1.0 \text{ min}^{-1}$. After inhaling room air to stabilize endogenous substance in their exhaled air, subjects inhaled test air containing one of ten organic soluble gases for 10 min and then switched to inhaling room air for 5 min. Throughout the 15 min experiment, mixed exhaled air was collected for an entire minute using a Tedlar bag and then analyzed. The bags were exchanged for another every minute. Breath-to-breath end-exhaled gas concentrations were measured and averaged over each 20 s period throughout the 15 min experiment. Both the mixed exhaled and end-exhaled gas concentrations were normalized by the inspired soluble gas concentration. After 8 min of washin, the mixed-exhaled and end-exhaled concentrations of these soluble gases reached a steady-state plateau.

Simulated Steady-State Washin. Of the ten gases studied by Kumagai *et al.*,²⁹ the steady-state uptake of seven were modeled. They are listed with their blood:air and water:air partition coefficients in Table 2. Three soluble gases were not modeled in this investigation because two were metabolized within the airways and another gas caused throat irritation during exposure. The final 2 min of mixed-exhaled, E_{mix} , and end-exhaled, E_{end} , washin data from Kumagai²⁹ were modeled as if

TABLE 2. Literature values for blood:air and water:air partition and temperature coefficients (%/°C) of twelve soluble gases at 37 °C.

Solvent	Partition and Temperature Coefficient			
	$\lambda_{b:a}$	$\alpha_{b:a}$	$\lambda_{w:a}$	$\alpha_{w:a}$
Ethane	0.088	-5.0	0.036 ^a	-2.1 ^a
Cyclopropane	0.36 ^b	-6.2 ^b	0.23 ^a	-1.7 ^a
Halothane	2.4 ^b	-3.7 ^b	0.7 ^b	-5.0 ^b
Ether	15.2 ^c	-3.8 ^c	16 ^c	-4.1 ^c
Methyl isobutyl ketone ¹	90 ^d	-5.0	79 ^d	-6.7 ^{d,e}
Methyl propyl ketone ¹	150 ^d	-5.0	166 ^d	-5.7 ^{d,e}
Acetone ¹	341 ^f	-5.5 ^f	279 ^f	-5.5 ^f
isoPropanol ¹	848 ^g	-5.0	1500 ^g	-3.2 ^{g,h}
Ethanol	1756 ⁱ	-6.7 ⁱ	2132 ⁱ	-6.4 ⁱ
Methanol ¹	2709 ^j	-5.9 ^j	3400 ^j	-2.9 ^j
Ethylene glycol monobutyl ether ¹	7970 ^k	-5.0	7050 ^k	-5.0
Propylene glycol monomethyl ether ¹	12380 ^k	-5.0	12280 ^k	-5.0

All values not referenced were assumed.

¹Soluble gas used in the Kumagai *et al.*²⁹ study.

^aWilhelm.⁴⁹

^bLowe.³²

^cEger.⁹

^dSato and Nakajima.³⁴

^eYaws *et al.*⁵²

^fWagner.⁴⁵

^gKaneko *et al.*²⁷

^hYaws *et al.*⁵¹

ⁱJones.²⁴

^jJones.²⁶

^kJohanson and Dynesius.²³

the data were in a steady state because the time course of the E_{mix} and E_{end} data show these two measures reaching a plateau at approximately the eighth minute of exposure. Additionally, the venous concentration of inert gas was assumed to be zero because of the high $\lambda_{b:a}$ of the gases used in the experiment.²⁸ Incorporating these two assumptions into the current model, the temperature and concentrations within the mathematical model were brought to steady state as outlined in the *Simulating Steady-state Gas Exchange* except a respiratory rate of 13 breaths per minute was used and a single soluble gas entered the lung via the inspired air. The end-exhaled and mixed-exhaled concentrations of soluble gas were calculated from the 31st simulated breath. The bronchial blood flow, \dot{Q}_{br} , was used as an adjustable parameter to fit the model predicted E_{mix} and E_{end} to the experimental values. The accuracy of this fit was determined by calculating the percent difference between the model predicted values and the experimental values for each soluble gas. The optimal fit and associated \dot{Q}_{br} was established by minimizing the sum of the absolute percent difference for E_{mix} and the absolute percent difference for E_{end} . The optimal blood flow was determined to within 0.1 ml s^{-1} .

PREDICTING LOCATION OF PULMONARY GAS EXCHANGE

While investigations have shown experimentally and mathematically that low blood-soluble gases ($\lambda_{b:a} < 10$) exchange largely in the alveoli and high blood-soluble gases ($\lambda_{b:a} > 1000$) exchange in the airways, an experimental or theoretical study has not demonstrated how intermediate blood-soluble gases ($10 < \lambda_{b:a} < 1000$) partition their exchange between the airways and alveoli. Here, this newly expanded and validated model of pulmonary gas exchange was used to predict the location and extent of low, intermediate, and high blood-soluble gas exchange in normal lungs during tidal breathing.

The model simulated the exchange of ten gases with $\lambda_{b:a}$ ranging between 0.088 and 2709 (Table 2) from lungs breathing tidally. Before simulating a tidal breath, the mathematical model was brought to steady state as outlined in the *Simulating Steady-State Gas Exchange*. For each simulation, a single soluble gas entered the lung via the pulmonary circulation and bronchial blood flow was set at 1 ml s^{-1} . To evaluate where each gas exchanged in the lung and to provide insight into the mechanisms of their exchange, three model outputs were

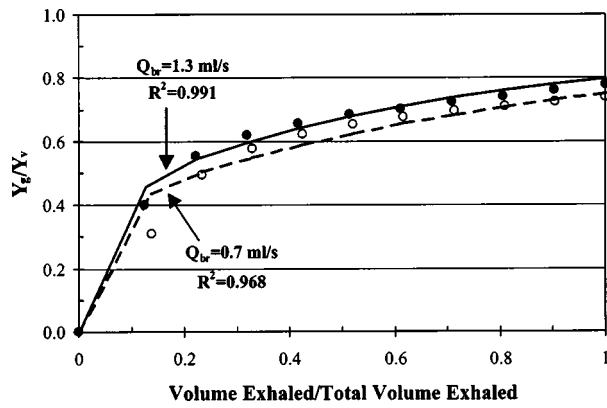


FIGURE 2. Experimental and model-predicted exhaled ethanol profiles for maneuver A and maneuver B for a representative subject (subject 5). Experimental data are designated by solid circles (●) for maneuver A and open circles (○) for maneuver B. Model-predicted profiles are shown using a solid line for maneuver A and a dashed line for maneuver B. The model fit to the data was optimized by adjusting the bronchial blood flow rate, \dot{Q}_{br} .

examined for each soluble gas: (1) the ratio of the net airway gas transfer to total pulmonary gas transfer [Eq. (10)]; (2) the axial distribution of soluble gas flux; and (3) the exhaled expirograms.

RESULTS

Validation—Ethanol Expirograms. The best-fit model predictions of the experimental ethanol expirograms from a representative subject (subject No. 5) for the slow exhalation and rapid exhalation maneuver are shown in Fig. 2. For this subject, the model required a bronchial blood flow of 1.3 and 0.7 ml s⁻¹ to accurately predict the expirograms for maneuver A and B, respectively. For each maneuver and subject, the best-fit values of \dot{Q}_{br} and R^2 are summarized in Table 3. For all six subjects, the

TABLE 3. Bronchial blood flows (ml s⁻¹) corresponding to the best-fit model predictions of the experimental exhaled ethanol data collected by George *et al.*¹³

Subject	Maneuver A		Maneuver B	
	\dot{Q}_{br}	R^2	\dot{Q}_{br}	R^2
1	0.1	0.990	0.1	0.822
2	0.1	0.950	0.1	0.888
3	0.8	0.981	0.5	0.979
4	1.5	0.992	0.6	0.946
5	1.3	0.991	0.7	0.968
6	1.6	0.996	1.1	0.994
Mean	0.9 [§]	0.983	0.5	0.933
SD	0.7	0.017	0.4	0.066

[§]Statistical difference between maneuver A and maneuver B ($p < 0.05$).

mean \dot{Q}_{br} and R^2 were 0.9 ml s⁻¹ and 0.983 for maneuver A and 0.5 ml s⁻¹ and 0.933 for maneuver B. Between maneuvers, the mean R^2 was statistically similar but the mean \dot{Q}_{br} was statistically different. When both maneuvers were combined, the mean \dot{Q}_{br} and R^2 were 0.7 ml s⁻¹ and 0.958.

The axial distribution of ethanol transport from the airway wall to the lumen as predicted by the current model are shown in Fig. 3(a). This transport of ethanol per generation during inspiration, j_{insp} , and expiration, j_{exp} , are presented for maneuver A from subject 5. A positive value indicates absorption of ethanol from the mucus to the airstream. A negative value denotes desorption of ethanol from the airstream to the mucus. Independent of maneuver, the axial distribution of ethanol transport on inspiration shows a bimodal distribution with a small peak in the trachea and larger peak at the 12th generation. After the 12th generation, j_{insp} for ethanol decreases until the alveolar region where it is nearly zero. Similar to the results of a previous study,⁶ almost 100% of ethanol exchange occurs completely within the airways.

In the current model, between 50% and 70% of the ethanol absorbed from the mucous layer on inspiration is deposited back to the airways on exhalation. This absorption–desorption phenomenon is similar to predictions made by previous airway gas exchange models^{6,13,43} and is the mechanism responsible for the phase III slope of the ethanol expirogram (see Discussion).

The axial distribution of water and heat transport from the airway wall to the lumen are shown in Figs. 3(b) and 3(c), respectively. Like the distribution of ethanol transport, the distribution of water and energy transport is bimodal with a large peak in the trachea and a smaller peak at the sixth generation. Heating and humidification of inspired air is nearly complete at generation 14 where almost no transport of water and energy between the wall and lumen occurs. Notice that the shape of the axial distribution of heat transport is almost identical to the distribution of water transport. These distributions are similar because of the highly coupled nature of these two quantities. In fact, 80% of the total energy transported is because of the latent heat effects of water.⁴³

Validation—Uptake of Soluble Gas. The current model was able to accurately predict the values of E_{mix} and E_{end} as measured by Kumagai *et al.*²⁹ by adjusting the bronchial blood flow rate. These results have been summarized in Table 4. The blood flow for ethylene glycol monobutyl ether was removed from the analysis as it was greater than two standard deviations from the mean. On average for the gases, the model overpredicted E_{mix} by 11% but predicted E_{end} to less than 0.1% accuracy.

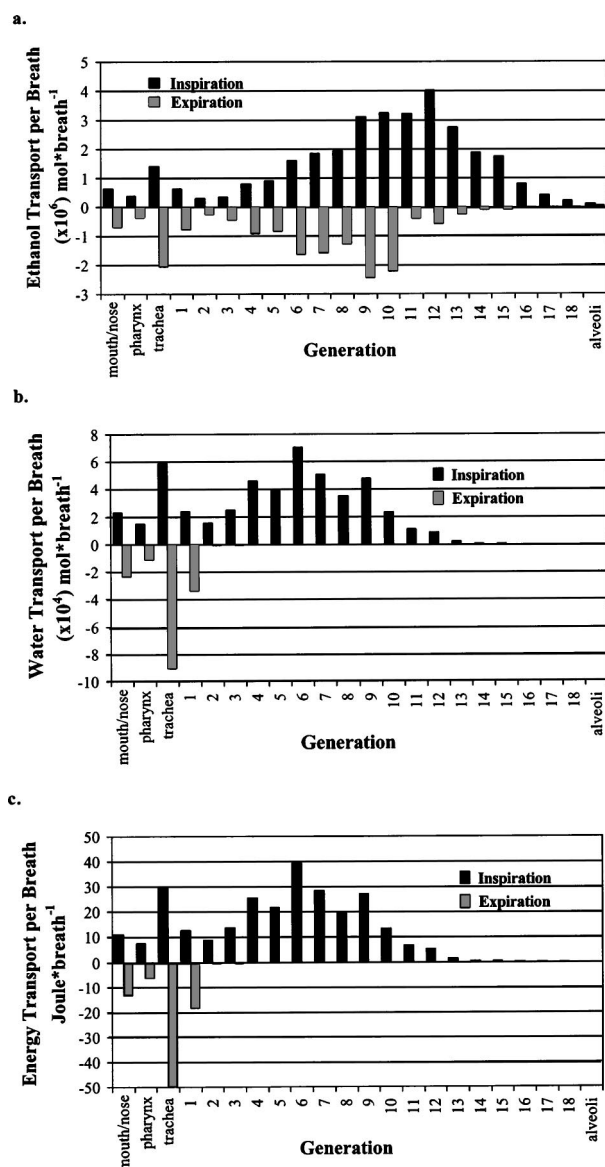


FIGURE 3. Axial distribution of ethanol (panel a), water (panel b), and energy (panel c) transport from the airway wall to lumen over one inspiration (black columns) and expiration (gray columns) for maneuver A. Ethanol transport (panel a) has a bimodal distribution with peaks in the trachea and generations 10–12. The shape of the axial distribution of heat transport is very similar to the distribution of water transport since 80% of the total energy transported results from latent heat effects.⁴³

The model was unable to predict the exchange of the extreme blood-soluble gas ethylene glycol monobutyl ether and had difficulty predicting E_{mix} for the other extreme blood-soluble gas propylene glycol monomethyl ether.

Predicting Pulmonary Gas Exchange Location. Because of the mathematical nature of our model, parameters that may be impossible to measure experimentally can be

TABLE 4. Bronchial blood flows corresponding to the best-fit model predictions of the steady-state uptake of seven soluble gases.²⁹

Soluble gas	\dot{Q}_{br}	% Difference E_{mix}	% Difference E_{end}
Methyl isobutyl ketone	4.0	-2.6	0.2
Methyl propyl ketone	1.1	-11.5	0.1
Acetone	1.6	-11.1	0.3
isoPropanol	2.2	-10.5	-0.1
Methanol	1.7	1.7	-0.2
Ethylene glycol monobutyl ether	*		
Propylene glycol monomethyl ether	3	-34.5	0.0
Mean	2.3	-11.4	0.0
SD	1.1	12.5	0.2

*Data point deleted from analysis as outlier (>2 SD from the mean).

calculated. The ratio of airway gas exchange to total pulmonary gas exchange can be calculated to determine the location of soluble gas exchange within the lung [Eq. (10)]. The ratio of airway gas exchange to total pulmonary gas exchange as a function of the blood:air partition coefficient has been plotted in Fig. 4. This figure demonstrates where the majority of gas exchange takes place for a range of blood-soluble gases. Soluble gases with a blood:air partition coefficient less than ten ($\lambda_{b:a} < 10$) exchange almost solely with the alveoli whereas gases with a blood:air partition coefficient greater than 100 ($\lambda_{b:a} > 100$) exchange almost exclusively with the airways. Gases in between these two extremes ($10 < \lambda_{b:a} < 100$) exchange partially with the airways and partially with the alveoli.

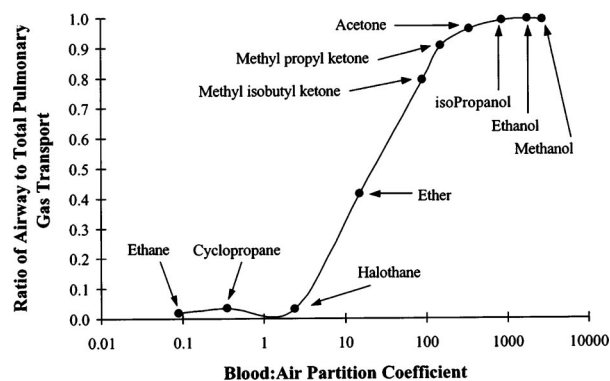


FIGURE 4. Ratio of airway gas exchange to total pulmonary gas exchange [Eq. (10)] is plotted vs. $\lambda_{b:a}$ for ten soluble gases as calculated from the airway–alveolar gas exchange model during tidal breathing. Greater than 95% of ethane, cyclopropane, and halothane gas exchange in the alveoli. The exchange of ether is partitioned equally between the airway and alveoli. Acetone and gases with a $\lambda_{b:a}$ greater than acetone exchange completely in the airways.

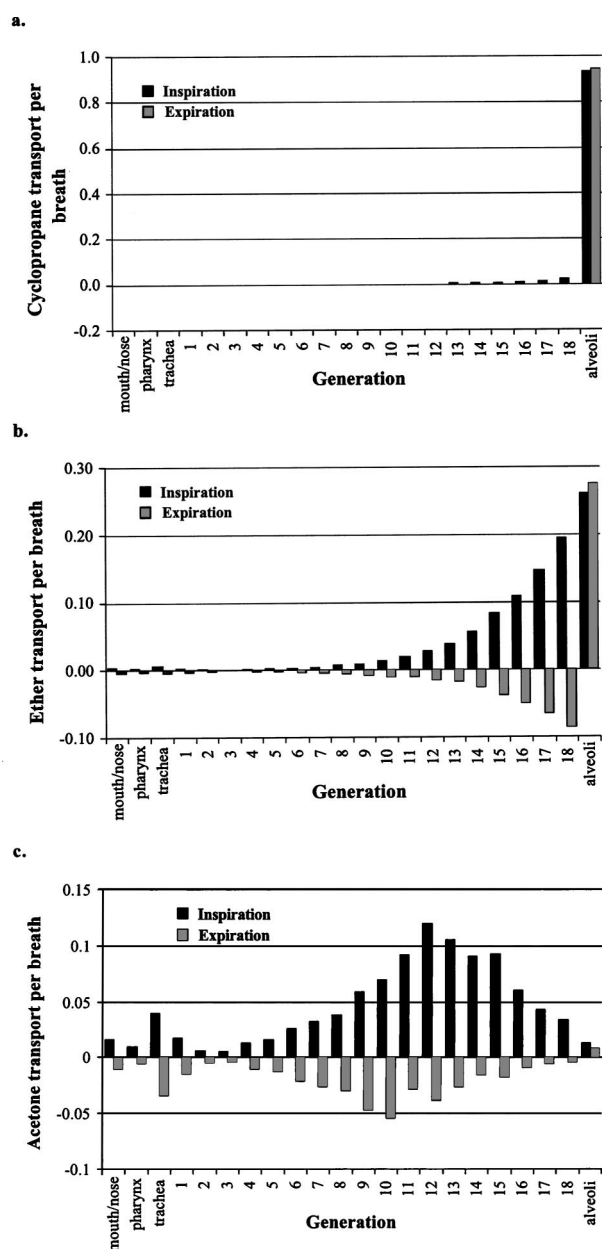


FIGURE 5. Axial distribution of gas transport during inspiration (black columns) and expiration (gray columns) for a tidal breath of cyclopropane (panel A), ether (panel B), and acetone (panel C). Each flux has been normalized by the total inspiratory soluble gas flux. As the blood solubility of gas increases from cyclopropane to acetone, the distribution shifts from a sharp concentrated peak in the alveolar region for cyclopropane to a wider distribution that spreads throughout the airways for acetone.

Another perspective on location and extent of gas exchange can be achieved by examining the axial distribution of gas transport from the airway lumen to mucus. Model predictions of these gas fluxes during inspiration, j_{insp} , and expiration, j_{exp} , are presented for cyclopropane, ether, and acetone in Figs. 5(A), 5(B), and 5(C), respectively. For cyclopropane, the flux distribution

shows a large peak in the alveoli that is an order of magnitude larger than the next largest flux [Fig. 5(A)]. Ether exchanges both in the airways and the alveoli (Fig. 4) and its flux profile illustrates this result. The largest flux of ether occurs in the alveoli; however, this flux is similar in size to the next largest flux occurring in generation 18 [Fig. 5(B)]. Ether has a greater spread in its flux distribution than cyclopropane. The flux profile for acetone [Fig. 5(C)] shows a bimodal distribution similar to that for ethanol (Fig. 3) with a small peak in the trachea and a large peak at generation 15. Unlike cyclopropane but similar to ether, all of the fluxes in the acetone distribution are within the same order of magnitude. However, the spread in the acetone flux distribution is larger than that for ether. In general, the results from Fig. 5 show that as the blood:air partition coefficient increases the flux profile shifts from being a concentrated spike in the alveoli to a more uniform distribution of fluxes spread throughout the airways.

The model's performance and its mechanisms of gas exchange were qualitatively evaluated by examining expirograms from tidal breathing. The expirograms of eight gases have been grouped and plotted according to their location of exchange. Gases with ($\lambda_{b:a} < 15$) exchange mostly in the alveoli and are plotted in Fig. 6(a) while gases with ($\lambda_{b:a} > 15$) exchange mainly in airways and are plotted in Fig. 6(b). Each expirogram has three distinct phases. These phases have been labeled on the cyclopropane expirogram [Fig. 6(a)]. Phase I represents the delay in the rise of soluble gas concentration as the volume of dead space is emptied. Phase II is the transition from dead space to exchange space, and phase III represents the emptying of the exchange space.

Three trends are predicted by the model as based on the soluble gas expirograms. First, phase I volume remains at $\sim 20\%$ of the exhaled volume for gases with $\lambda_{b:a} < 15$. For gases with $\lambda_{b:a} > 15$, the phase I volume decreases to $\sim 10\%$ for acetone ($\lambda_{b:a} = 341$) and $\sim 5\%$ for methanol ($\lambda_{b:a} = 2709$) as $\lambda_{b:a}$ increases. Second, the model predicts that the phase III slope is slightly positive for soluble gases with $\lambda_{b:a} < 15$. For gases with $15 < \lambda_{b:a} < 341$, the phase III slope is more positive but decreases in value as $\lambda_{b:a}$ increases above $\lambda_{b:a} = 341$. Third, the model predicts that E_{end} increases as $\lambda_{b:a}$ increases to 15 and then E_{end} decreases as $\lambda_{b:a}$ increases past 15.

DISCUSSION

Model Validation

The current model of heat, mass, and soluble gas transport in the airways and alveoli was fit to two sets of data by using \dot{Q}_{br} as the free parameter. The model accurately predicted 12 ethanol expirograms using

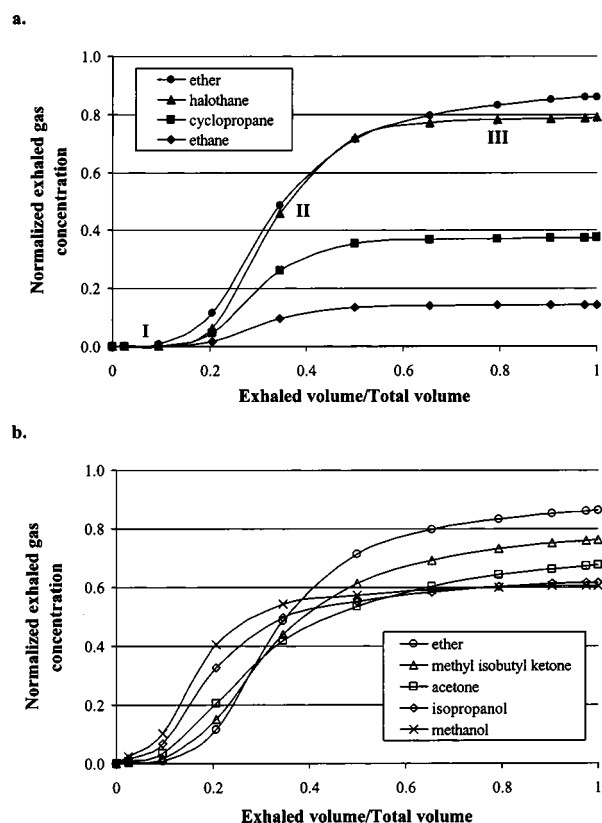


FIGURE 6. Expirograms for tidal breaths of soluble gas that exchange mainly in the alveoli (panel A) and airways (panel B). The curves in panel A show $\sim 30\%$ dead space and end-exhaled concentrations that increase with blood solubility. Panel B curves show that both dead space and end-exhaled concentration decrease with increasing blood solubility.

mean best-fit values of \dot{Q}_{br} and R^2 , 0.7 ml s^{-1} and 0.958 . The model was further optimized with a short duration washin of seven soluble gases. The model predicted E_{mix} and E_{end} for six of the seven gases to within 11% and 0.1% of the experimental measurements and required a mean \dot{Q}_{br} of 2.3 ml s^{-1} .

Although different, the \dot{Q}_{br} required by the model to optimally predict the two sets of experimental data compares favorably with measured values in the literature. If the average cardiac output is assumed to be 61 min^{-1} (100 ml s^{-1}), the mean bronchial blood flow for the ethanol data and the uptake data as predicted by the current model is approximately 0.7% and 2.3% of cardiac output, respectively. The \dot{Q}_{br} predicted by our current model is within the range reported in the literature, namely, $1\%–3\%$ of cardiac output^{1,8} or $0.25–2 \text{ ml s}^{-1}$.^{4,8,33} Because of this variability in the measured value of \dot{Q}_{br} , the bronchial blood flow rate was chosen as the adjustable parameter to fit the model predicted values to the experimental data as described above. Additionally, by using \dot{Q}_{br} as the adjustable parameter for fitting the ex-

perimental data, the model implicitly demonstrated an experimental observation: airway gas exchange is dependent on airway perfusion.³⁹

A best-fit \dot{Q}_{br} was found to fit the model predictions to the ethanol expirograms for each subject and maneuver. The mean best-fit \dot{Q}_{br} across subjects for maneuver A was found to be significantly different ($p = 0.045$) than the mean best-fit \dot{Q}_{br} for maneuver B as determined by a two-tailed t test (Table 3). However within each subject, the difference in \dot{Q}_{br} between maneuvers was relatively small. To determine if this difference in \dot{Q}_{br} between maneuvers resulted in decreased accuracy of predictions made by the current model, we calculated the average best-fit \dot{Q}_{br} for each subject. For example, the average best-fit \dot{Q}_{br} for subject 5 was 1.0 ml s^{-1} . Then, with the current model, we simulated both exhalation maneuvers (A and B) for each subject using a single bronchial blood flow, the subject's average best-fit \dot{Q}_{br} . Using these conditions, the current model predicted the exhalation profiles from subjects 3–6 with slightly less accuracy (as measured by R^2) than the best-fit predictions. The average change in R^2 from the best-fit predictions was 0.01 for subjects 3–6. For all six subjects, the mean R^2 was 0.978 for maneuver A and 0.925 for maneuver B. We concluded that the difference in the mean \dot{Q}_{br} between maneuvers, although statistically significant, was relatively insignificant in terms of the predictive ability of the current model.

To predict the uptake of soluble gas, the model required an average \dot{Q}_{br} of 2.1 ml s^{-1} to accurately predict E_{end} and E_{mix} of the first five soluble gases up to and including methanol. Using the optimal \dot{Q}_{br} , the model predicted E_{end} to within 0.1% and E_{mix} to within 11% . For all the fitting exercises, the model always predicted E_{end} more precisely than E_{mix} because E_{end} was more sensitive to changes in \dot{Q}_{br} . As a result, minimizing the difference between the predicted and experimental E_{end} was very important to fit the model. The model had difficulty predicting the experimental data of the extremely soluble gases: ethylene glycol monobutyl ether (EGME) and propylene glycol monomethyl ether (PGME). From examining the data of Kumagai, it is possible that these two gases were not in a steady state. Because their blood:air partition coefficient is $3–5$ times larger than methyl alcohol which only just reached a steady-state plateau within 10 min , these gases may have needed to be inhaled for a few more minutes in order to reach a steady state. Additionally, the lung volume of each subject was not reported by Kumagai but may be important for predicting the exchange of these gases. Hlastala¹⁹ has hypothesized that the lung volume of a subject may affect the exhaled concentrations of soluble gases that exchange solely in the airways. Even with

these concerns, it is important to remember that the model was able to accurately predict the exchange of gases with $90 < \lambda_{b:a} < 2709$. This validation positioned the model to make accurate predictions of gas exchange location (airway versus alveolar) within the lung.

Diffusing Capacity

Airway gas exchange has been shown to be dependent on the molecular diffusion of soluble gas through the airway tissue.^{13,40} This diffusion dependence is best understood by examining the diffusing capacity of the airway tissue, D_L :

$$D_L = \frac{D_t \Phi_c A_s}{\ell_t}.$$

This diffusing capacity is a function of the molecular diffusion coefficient through tissue, D_t , the surface area for diffusion between the capillary and tissue which is represented by the capillary area fraction, Φ_c , multiplied by the airway surface area, A_s , and divided by the connective tissue thickness, ℓ_t . In previous model studies of airway gas exchange, the diffusing capacity was incompletely specified. One goal of the current study was to accurately specify the tissue diffusing capacity and incorporate it into our model of airway gas exchange.

One factor, the molecular diffusion coefficient, describes how easily a molecule can diffuse through a medium. The larger the coefficient the faster a molecule can travel through the medium. Because of the heterogeneous structure of tissue, many small molecules have lower diffusion coefficients in tissue relative to water. The diffusion coefficient of ethanol in the respiratory tissue was measured and found to be 33% of its value in water.¹² As a result, the diffusion coefficient for ethanol is fairly well quantified.

Values for the other two factors, the capillary surface area, $\Phi_c A_s$, and connective tissue thickness, ℓ_t , were unknown. Recently, these values were measured in sheep by Anderson *et al.*³ Since A_s can be calculated easily, only the capillary area fraction, Φ_c , needed to be determined. The capillary area fraction was found to be independent of airway diameter and equal to 0.58. However, only half of that, 0.29, participates in exchange with the airway lumen. The connective tissue thickness, ℓ_t , was measured, scaled to simulate human airways, and was found to range from 160 μm in the trachea to 30 μm in the bronchioles. Accurately specifying the diffusing capacity is an important reason why the model was able to accurately predict the experimental data using realistic values of \dot{Q}_{br} .

Adventitial Layer

A major improvement to the current model was the inclusion of experimental measurements on the airway wall and bronchial circulation. These measurements allowed the addition of an adventitial layer and an adjacent pulmonary layer to the model. However, we felt these layers should not be included at every airway generation for the following reasons.

In the extrapulmonary airways (mouth to second generation), the adventitial and pulmonary layers were not included because anatomical measurements and physiological data for analogous structures in the extrapulmonary airways were unavailable. For the current model and study, the extrapulmonary airways play a significant role in the exchange of energy and water [Figs. 3(b) and 3(c)]. We feel the essence of this exchange has been captured by the current model without the inclusion of these adventitial and pulmonary layers: (1) our axial distributions of energy and water transport during a prolonged exhalation [Figs. 3(b) and 3(c)] compare nicely with a similar model of airway exchange;⁶ (2) the mean end-exhaled temperature for our model simulations (35.6 °C) is very similar to that measured under similar conditions (34.6 °C);²⁵ and (3) the current model accurately predicts the exchange of ethanol which has a blood and water solubility that is strongly dependent on temperature.²⁴

For airways beyond the second generation (intraparenchymal airways), the adventitial and pulmonary layers were included. For airway generations three through ten, cartilage is present in the adventitial layer.²⁰ Gerde *et al.*¹⁵ in their model of toxicant absorption by the airway wall assumed the cartilage was an impermeable barrier to gas transport. As a result, we assumed the cartilage in this layer presented a significant barrier to soluble gas transport. Data on the diffusivity of soluble gas through cartilage were unavailable. Consequently, we assumed that the molecular diffusivity of soluble gas through the adventitial layer to be 10% of the molecular diffusivity through the connective tissue (i.e., ~3% of the molecular diffusion coefficient of soluble gas through water). Without this assumption, the model overpredicted the ethanol expirograms of subjects 1 and 2. Since cartilage is assumed to be a major barrier to the diffusion of soluble gas from the pulmonary layer to the airway lumen in the current model, the major function of the adventitial and pulmonary layers in airway generations three through ten for this model is thermoregulation. Figures 3(b) and 3(c) show that these airway generations participate significantly in the exchange of energy and water which is a result of the pulmonary layer's participation in energy exchange. This finding that the pulmonary circulation participates in airway energy exchange reinforces an experimental investigation demonstrating

the prominent role of the pulmonary circulation in the thermoregulation of the airways.³⁸

For airway generations greater than ten, the adventitial and pulmonary layers were included without any deviation from that presented in the model description and shown in Fig. 1. Here, the alveoli lie in close proximity to the intraparenchymal airways. These layers participate mostly in soluble gas exchange with the bronchial circulation or connective tissue as the inspired air is completely heated and humidified by the time it reaches these airways.

Solubility Dependence on Temperature

We know that $\lambda_{b:a}$ of a soluble gas is the most important factor for determining the location of pulmonary gas exchange. However, $\lambda_{b:a}$ depends strongly on temperature (Table 2) which can range from 23 °C in the mouth to 37 °C in the alveoli. Over this range, the blood–air partition coefficient can vary considerably. For example, ethanol's temperature coefficient for $\lambda_{b:a}$ is $-6.7\%/^{\circ}\text{C}$.²⁴ As a result, $\lambda_{b:a}$ for ethanol at the mouth ($T=23^{\circ}\text{C}$) can be 150% larger than $\lambda_{b:a}$ for ethanol in the alveoli ($T=37^{\circ}\text{C}$). The dependence of $\lambda_{b:a}$ on temperature primarily affects soluble gas exchange that takes place in the same airways that heat and humidify inspired air. In these airways, a large axial temperature gradient is present that will change the value of $\lambda_{b:a}$. When breathing room air at rest, this dependency will most likely only affect soluble gases with $\lambda_{b:a} > 800$ like ethanol that primarily exchange in the first ten airway generations. However, during exercise or breathing cold-dry air, a greater number of airway generations participate in heating and humidifying inspired air. As a result, the exchange of soluble gases with much smaller $\lambda_{b:a}(T=37^{\circ}\text{C})$ values than isopropanol will be significantly influenced by the axial temperature gradient. To account for this temperature effect on airway gas exchange, the current model of pulmonary gas exchange includes a description of energy exchange which, in turn, places the model in a strong position to study the effects of inspired air conditions and exercise on pulmonary gas exchange.

Location of Gas Exchange

Figure 6(a) shows that the model predicted expirograms of some low blood-soluble gases ($\lambda_{b:a} < 15$) have a phase I volume that is $\sim 20\%$ of the expired volume, a slightly positive phase III slope, and E_{end} that increases as blood solubility increases. These trends can be predicted from classical respiratory physiology because these gases exchange solely in the alveoli and do not interact with the airways. On exhalation, air in the respiratory tract does not contain soluble gas and leaves the lung before the alveolar air. This volume of nonexchang-

ing air is represented by phase I on the expirogram. Here, the concentration of soluble gas is zero in the first $\sim 20\%$ of the expirate. In addition to phase I, the phase III slope of a low blood-soluble gas is thought to result from ventilation/volume effects, a longitudinal stratification of soluble gas in the alveolar region, and continuing gas exchange.³⁷ Because the model has a symmetrical airway structure and the alveolar space is modeled as a well-mixed compartment, the small positive phase III slope for these gases as predicted by the model must result from continuing gas exchange, the transport of soluble gas from the pulmonary blood into the contracting alveolar compartment. At the end of phase III is E_{end} which increases as blood solubility increases. E_{end} is representative of the alveolar gas concentration and as such, this trend can be predicted by the alveolar gas exchange kernel developed by Farhi¹⁰ [$E = \lambda_{b:a} / (\lambda_{b:a} + \dot{V}_A / \dot{Q}_p)$].

Before examining the model predicted expirograms of the high blood-soluble gases ($15 > \lambda_{b:a} > 2700$) that primarily exchange with the airways [Fig. 6(b)], it is helpful to briefly describe the mechanisms of airway gas exchange. As fresh air is inspired, this air absorbs soluble gas from the mucous layer thereby depleting the soluble gas concentration in the airway wall. Because the small bronchial blood flow and the significant tissue barrier between the bronchial circulation and mucus layer, the mucus is not replenished with soluble gas before expiration begins. During expiration, the air encounters a lower concentration of soluble gas in the mucus and therefore a larger driving force for the redeposition of soluble gas on the mucus. This large air-to-mucus gradient promotes recovery of soluble gas by the mucous layer and delays the rise in soluble gas concentration at the mouth, thus accounting for the steep phase III slope. These absorption–desorption phenomena decrease the amount of soluble gas leaving the lung late in exhalation and is the major mechanism of pulmonary gas exchange when $\lambda_{b:a} > 100$.

Examining the expirograms from Fig. 6(b), the model predicts the following for these high blood-soluble gases: the phase I volume decreases with increases in $\lambda_{b:a}$, the phase III slope is strongly positive, and E_{end} decreases as blood solubility increases. First, the air in the conducting airways contains soluble gas and thus the airways are considered part of the exchange space. As a result, the volume of nonexchanging air (phase I) which originates in the airways is less than that for gases with $\lambda_{b:a} < 15$. As blood-solubility increases, the phase I volume decreases because more proximal airways participate in a larger portion of gas exchange. This result is nicely demonstrated in Fig. 5 where the axial distribution of gas exchange moves towards the proximal airways as $\lambda_{b:a}$ increases from cyclopropane to acetone. In addition to this model prediction, experimental observations have

reported that these soluble gases appear in the expirate earlier than gases of low-blood solubility.^{13,36} Second, the positive phase III slope of these gases reflects the temporal exchange mechanism described above and by George *et al.*¹³ The model predicts the phase III slope decreases for gases with $\lambda_{b:a} \sim 800$ (isopropanol) and larger. This result coincides with the appearance of a large soluble gas flux in the trachea [compare Fig. 3(a) to 5(c)] and might simply imply that the phase III slope decreases as the majority of gas exchange occurs in the more proximal airways. Third, the model predicts E_{end} of these gases to be inversely proportional to the blood solubility. This trend is caused by the absorption-desorption phenomena which decrease the amount of soluble gas leaving the lung late in exhalation and causes the end-exhaled concentration of soluble gas to be less than its alveolar concentration. This finding was suggested by Schrikker *et al.*³⁵

Intermediate Soluble Gas Exchange

Figure 4 shows that soluble gases with $10 < \lambda_{b:a} < 100$ exchange partially with the airways and partially with the alveoli. The gases that lie within these two extremes, the intermediate soluble gases, are encountered daily and monitored as a result of their importance in the biological, medical and occupational venues. Toluene, diethyl ether, and methyl isobutyl ketone are all solvents but are also used as a gasoline component, anesthetic, and lacquer, respectively. Because these intermediate soluble gases interact with both the airways and alveoli, the exchange of these intermediate soluble gases is likely dependent on both alveolar and airway gas exchange mechanisms: alveolar ventilation, pulmonary perfusion, bronchial perfusion, and the diffusing capacity of the airway tissue. The influence of these factors on intermediate soluble gas exchange may vary depending on the spatial heterogeneity of these factors within a subject and the temperature and water concentration of the inspired air. Consequently, we may have to reevaluate how the exchange of these gases are interpreted. In particular, the multiple inert gas elimination technique relies on diethyl ether to quantify heterogeneity of alveolar ventilation and perfusion.⁴⁶ This measure of heterogeneity may be affected by changes in airway tissue thickness, bronchial blood flow, or inspired air conditions—factors that impact airway gas exchange. Conversely, an understanding of the exchange of these gases in normal subjects in conjunction with our current knowledge of low and high soluble gas exchange should provide new insights into secondary factors that determine pulmonary gas exchange. Perhaps such new information on intermediate soluble gas exchange will lead to tests that focus on these gases to more accurately predict the exchange efficiency and health of the airways and alveoli.

CONCLUSIONS

A mathematical model of heat, water, and soluble gas exchange in the airways was improved by incorporating anatomical data on the airway wall and expanding the model to include a time varying alveolar compartment. The model was tested using experimental ethanol expirograms and the uptake of seven soluble gases from human subjects. To accurately predict these data, the model required a bronchial blood flow that is similar to the experimentally measured values of bronchial blood flow in humans. The model was used to predict gas exchange location in the lung (airways versus alveoli) and found that gases with a blood:air partition coefficient, $\lambda_{b:a}$, less than 10 exchange almost solely in the alveoli and gases with $\lambda_{b:a} > 100$ exchange almost exclusively in the airways. Gases with $\lambda_{b:a}$ between 10 and 100 have significant interaction with the airways and alveoli. Many more soluble gases than previously thought exchange primarily in the airways. The exchange of these gases may be affected by inspired air conditions and bronchial blood flow. The exchange of soluble gases that interact with both the airways and alveoli will be affected to varying degrees by all pulmonary gas exchange mechanisms. In general, these results suggest that the airways play a larger role in pulmonary gas exchange than previously assumed and we may need to reevaluate the implications of pulmonary tests employing soluble gases with $\lambda_{b:a} > 10$.

ACKNOWLEDGMENT

This work was supported, in part, by Grant No. HL24163 from the National Heart, Lung, and Blood Institute.

APPENDIX

The equations describing the transport of mass and energy in each radial compartment are briefly described and presented below. Derivation of the equations are not presented as the methodology is similar to the control volume approach used by Tsu *et al.*⁴² For each compartment, the volume is assumed to be constant with the exception of the mucous layer. The gas in the airway lumen is assumed to behave like an ideal gas so that $C_g = P_t / (RT_{\text{ABS}})$ where P_t is the total pressure, R is the gas constant, and T_{ABS} is the airway temperature in Kelvin ($= T_a + 273.15$). The total molar concentration, C , in each radial compartment is assumed to be equal to that of water and can be expressed as $C = \rho / M_w$ where ρ is the density of water and M_w is the molecular weight of water. The molar concentration of soluble gas in each radial layer is expressed as the mole fraction,

$X = C_a/C$. The mole fraction between radial compartments can be related using a partition coefficient, e.g., $X_t = \lambda_{t:m} X_m$.

Airway Lumen

Material Balance. The molar balance of a species i , either soluble gas or water, for a control volume (C.V.) in the airway lumen was described by Tsu *et al.*⁴² A term has been added to account for axial diffusion in the airway. Equation (A1) shows the accumulation of mass in the airway lumen to be equal to the convection of mass by ventilation, axial diffusion of mass, and molar evaporation of species i from the mucosal surface:

$$\begin{aligned} \left. \frac{\partial}{\partial t} (n_{\text{tot}} Y_i) \right|_{\text{C.V.}} = & -\dot{V} \left. \frac{\partial}{\partial z} (C_g Y_i) \right|_{\Delta z} \Delta z \\ & + \left. \frac{\partial}{\partial z} \left(A D_{a,i} \frac{\partial (C_g Y_i)}{\partial z} \right) \right|_{\Delta z} \Delta z + \dot{n}_i. \end{aligned} \quad (\text{A1})$$

The molar evaporation rate of species i can be expressed in terms of a local mass transfer coefficient and the mole fraction difference:

$$\dot{n}_i = A_s k_{y,i} [Y_{\text{wall},i} - Y_i]. \quad (\text{A2})$$

Substituting Eq. (A2) into (A1) and assuming n_{tot} and C_g have ideal gas behavior, the governing equation can be written for gas species i [i.e., water (subscript w) or soluble gas (subscript a)]:

$$\begin{aligned} \frac{\partial Y_i}{\partial t} = & \left(\frac{Y_i}{T_{\text{ABS}}} \right) \frac{\partial T_a}{\partial t} - \left(\frac{4\dot{V}}{\pi d^2} \right) \frac{\partial Y_i}{\partial z} + \left(\frac{4\dot{V}Y_i}{\pi d^2 T_{\text{ABS}}} \right) \frac{\partial T_a}{\partial z} \\ & + \left(\frac{4RT_{\text{ABS}}}{dP_t} \right) k_{y,i} [Y_{\text{wall},i} - Y_i] + D_{\text{axial},i}, \end{aligned} \quad (\text{A3})$$

where

$$\begin{aligned} D_{\text{axial},i} = & D_{a,i} \left[\frac{\partial^2 Y_i}{\partial z^2} - \frac{2}{T_{\text{ABS}}} \frac{\partial Y_i}{\partial z} \frac{\partial T_a}{\partial z} + \frac{2Y_i}{T_{\text{ABS}}^2} \left(\frac{\partial T_a}{\partial z} \right)^2 \right. \\ & \left. - \frac{Y_i}{T_{\text{ABS}}} \frac{\partial^2 T_a}{\partial z^2} \right]. \end{aligned}$$

Energy Balance. The accumulation of energy in the control volume is equal to the convection of energy by ventilation, conduction of energy from the mucus (i.e., sensible heating) and transportation of energy associated

with water vaporization/condensation (i.e., latent heating) and was initially described by Tsu *et al.*⁴²

$$\left. \frac{\partial E_{\text{tot}}}{\partial t} \right|_{\text{C.V.}} = - \left. \frac{\partial (n \bar{H}^g)}{\partial z} \right|_{\Delta z} \Delta z + \dot{Q}_{\text{sens}} + \sum_{i=1}^2 \dot{n}_i \bar{H}_i^g. \quad (\text{A4})$$

After simplification and substitution of Eq. (A3) into Eq. (A4), the governing equation is similar to that by Tsu *et al.*⁴² with an additional term ($D_{\text{axial},i}$) resulting from axial diffusion of soluble gas and water:

$$\begin{aligned} \frac{\partial T_a}{\partial t} = & - \frac{4\dot{V}}{\pi d^2} \frac{\partial T_a}{\partial z} + \frac{4RT_{\text{ABS}} h (T_m - T_a)}{dP_t} \\ & \frac{273.15}{T_{\text{ABS}}} \bar{C}_{p,da}^g + \sum_{i=1}^2 Y_i \Delta \bar{C}_{p,i}^g \\ & - \frac{\sum_{i=1}^2 D_{\text{axial},i} (\Delta \bar{C}_{p,i}^g T_a + \Delta \bar{H}_i^{\text{vap}})}{\frac{273.15}{T_{\text{ABS}}} \bar{C}_{p,da}^g + \sum_{i=1}^2 Y_i \Delta \bar{C}_{p,i}^g} \\ & + \frac{4RT_{\text{ABS}}}{dP_t} \sum_{i=1}^2 (\bar{C}_{p,da}^g T_a - \bar{C}_{p,i}^{\ell} T_m) k_{y,i} (Y_{\text{wall},i} - Y_i) \\ & + \frac{273.15}{T_{\text{ABS}}} \bar{C}_{p,da}^g + \sum_{i=1}^2 Y_i \Delta \bar{C}_{p,i}^g, \end{aligned} \quad (\text{A5})$$

where

$$\Delta \bar{C}_{p,a}^g = \bar{C}_{p,a}^g - \bar{C}_{p,da}^g, \quad \Delta \bar{C}_{p,w}^g = \bar{C}_{p,w}^g - \bar{C}_{p,da}^g$$

and

$$\Delta \bar{H}_a^{\text{vap}} = \bar{H}_a^{\text{vap}} - \bar{H}_{da}^{\text{vap}}, \quad \Delta \bar{H}_w^{\text{vap}} = \bar{H}_w^{\text{vap}} - \bar{H}_{da}^{\text{vap}}.$$

Mucus

Thickness of Layer. The governing equation for the thickness of the mucous layer is the same as the one derived by Tsu *et al.*⁴² The thickness of the mucous layer is assumed to be independent of airway curvature. The mucous layer thickness is decreased by evaporation of liquid but a minimum thickness is maintained by secretion of fluid from the bronchial bed into the layer via the connective tissue. The general equation describing thickness of the mucous layer can be written

$$A_s C \frac{\partial \ell_m}{\partial t} = A_s (\dot{S} - k_{y,a} [Y_{\text{wall},a} - Y_a] - k_{y,w} [Y_{\text{wall},w} - Y_w]). \quad (\text{A6})$$

This general equation is subject to two conditions that depend on the thickness of the mucous layer. These conditions result in the following two specific solutions used in the mathematical model.

When the mucous layer thickness is less than a minimum thickness, $\ell_m < \ell_{m,\min}$, the secretion rate is equal to the evaporation rate of liquid from the mucus to the lumen and the change in mucous layer per time can be written

$$\frac{\partial \ell_m}{\partial t} = 0. \quad (\text{A7})$$

When the mucous layer thickness is greater than a minimum thickness, $\ell_m > \ell_{m,\min}$, the secretion rate is equal to zero and the change in mucous layer per time can be written

$$\frac{\partial \ell_m}{\partial t} = -\frac{1}{C} (k_{y,a} [Y_{\text{wall},a} - Y_a] + k_{y,w} [Y_{\text{wall},w} - Y_w]). \quad (\text{A8})$$

Material Balance. The accumulation of mass in the mucous layer is equal to the diffusion of mass to the layer from the connective tissue, and transfer of mass from the layer to the airway lumen. When the mucous layer thickness falls below a minimum thickness, fluid is secreted from the bronchial bed into the layer via the connective tissue to maintain a minimum mucous thickness.

$$\begin{aligned} \frac{\partial X_m}{\partial t} = & \frac{D_m}{\frac{1}{2}(\ell_m + \ell_t)\ell_m} \left(\frac{X_t}{\lambda_{t:m}} - X_m \right) \\ & - \frac{1}{C\ell_m} \left(\frac{X_j}{\lambda_{j:m}} k_{y,w} [Y_{\text{wall},w} - Y_w] \right. \\ & \left. - \left(1 - \frac{X_j}{\lambda_{j:m}} \right) k_{y,a} [Y_{\text{wall},a} - Y_a] \right), \quad (\text{A9}) \end{aligned}$$

where $j = \text{mucous layer } (m)$ when $\dot{S} = 0$ (i.e., $\ell_m > \ell_{m,\min}$) and $j = \text{tissue layer } (t)$ when $\dot{S} > 0$ (i.e., $\ell_m < \ell_{m,\min}$).

Energy Balance. The accumulation of energy in the mucous layer is equal to the energy change associated with the changing mucous thickness, the conduction of energy to the layer from the connective tissue, transport of energy to the lumen resulting from convective and conductive effects, transport of energy associated with fluid

secretion from the connective tissue, and energy transport resulting from evaporation and condensation of water and soluble gas:

$$\begin{aligned} \frac{\partial T_m}{\partial t} = & -\frac{T_m}{\ell_m} \frac{\partial \ell_m}{\partial t} + \frac{k_{\text{th}}}{C\bar{C}_{p,w}^{\ell} \ell_m^{\frac{1}{2}} (\ell_m + \ell_t)} (T_t - T_m) \\ & - \frac{h}{C\bar{C}_{p,w}^{\ell} \ell_m} (T_m - T) - \frac{\dot{S} C_{p,t} T_t}{C\bar{C}_{p,w}^{\ell} \ell_m} - \frac{1}{C\bar{C}_{p,w}^{\ell} \ell_m} \\ & \times \sum_{i=1}^2 (\Delta H_i^{\text{vap}} - \bar{C}_{p,i}^{\ell} T_m + \bar{C}_{p,i}^g T_a) k_{y,i} (Y_{\text{wall},i} - Y_i). \quad (\text{A10}) \end{aligned}$$

Connective Tissue Layer

Material and Energy Balances. The accumulation of mass/energy in the connective tissue is equal to the diffusion of mass/energy to the layer from the adventitial layer and bronchial bed, diffusion of mass/energy from the layer to the mucous layer, and mass/energy transport via secretion of fluid into and out of the layer from the bronchial bed and to the mucous layer, respectively.

$$\begin{aligned} \frac{\partial X_t}{\partial t} = & \frac{(1 - \Phi_c) D_t}{\frac{1}{2}(\ell_{ad} + \ell_t)\ell_t} (X_{ad} - X_t) + \frac{\Phi_c D_t}{\frac{1}{2}\ell_t^2} \left(\frac{X_c}{\lambda_{b:t}} - X_t \right) \\ & - \frac{D_m}{\frac{1}{2}(\ell_m + \ell_t)\ell_t} (X_t - X_m \lambda_{t:m}) \\ & + \frac{\dot{S}}{\ell_t C} \left(\frac{X_c}{\lambda_{b:t}} - X_t \right), \quad (\text{A11}) \end{aligned}$$

$$\begin{aligned} \frac{\partial T_t}{\partial t} = & \frac{k_{\text{th}}}{\frac{1}{2}C\bar{C}_{p,t}^{\ell} \ell_t} \left[\frac{(1 - \Phi_c)(T_{ad} - T_t)}{(\ell_{ad} + \ell_t)} + \frac{\Phi_c(T_c - T_t)}{\ell_t} \right. \\ & \left. - \frac{(T_t - T_m)}{(\ell_m + \ell_t)} \right] + \frac{\dot{S}}{C\bar{C}_{p,t}^{\ell} \ell_t} (C_{p,b} T_c - C_{p,t} T_t). \quad (\text{A12}) \end{aligned}$$

Bronchial Bed

Material Balance. The mass balance describing soluble gas accumulation in the bronchial bed is similar to that derived by Bui *et al.*⁶ The accumulation of material in the bronchial bed is equal to the convection of mass via bronchial perfusion, diffusion of material into and out of the layer from the adventitia and to the connective tis-

sue, respectively, and transport of material via secretion to the connective tissue layer. A general material balance can be written

$$\begin{aligned} \frac{\partial(v_c CX_c)}{\partial t} &= \dot{q}_{br} CX_a - (\dot{q}_{br} - \dot{S}A_s) CX_c - \dot{S}A_s CX_c \\ &+ \frac{A_s \Phi_c CD_t}{\frac{1}{2}\ell_{ad}} (X_{ad}\lambda_{b:t} - X_c) \\ &- \frac{A_s \Phi_c CD_t}{\frac{1}{2}\ell_t} (X_c - X_t\lambda_{b:t}). \end{aligned} \quad (A13)$$

After simplification, the final form of the equation is:

$$\begin{aligned} \frac{\partial X_c}{\partial t} &= \frac{\dot{q}_{br}}{v_c} (X_a - X_c) + \frac{D_t A_s \Phi_c}{\frac{1}{2}\ell_{ad} v_c} (X_{ad}\lambda_{b:t} - X_c) \\ &- \frac{D_t A_s \Phi_c}{\frac{1}{2}\ell_t v_c} (X_c - X_t\lambda_{b:t}). \end{aligned} \quad (A14)$$

Energy Balance. The governing equation for the energy balance in the bronchial bed can be derived the same way as the material balance and may be written as follows:

$$\begin{aligned} \frac{\partial T_c}{\partial t} &= \frac{\dot{q}_{br}}{v_c} (T_b - T_c) + \frac{k_{th} A_s \Phi_c}{\frac{1}{2}v_c C \bar{C}_{p,b}^\ell} \\ &\times \left[\frac{(T_{ad} - T_c)}{\ell_{ad}} - \frac{(T_c - T_t)}{\ell_t} \right]. \end{aligned} \quad (A15)$$

Adventitial Layer

Material and Energy Balances. The accumulation of mass/energy in the adventitial layer is equal to the diffusion of mass/energy into the layer from the pulmonary bed, and from the layer to the connective tissue and bronchial bed via diffusion. These equations can be written as:

$$\begin{aligned} \frac{\partial X_{ad}}{\partial t} &= \frac{D_t A_s}{\frac{1}{2}\ell_{ad} v_{ad}} \left(\frac{X_p + X_c}{2\lambda_{b:t}} - X_{ad} \right) \\ &- \frac{D_t A_s \Phi_c}{\frac{1}{2}\ell_{ad} v_{ad}} \left(X_{ad} - \frac{X_c}{\lambda_{b:t}} \right) \\ &- \frac{D_t A_s (1 - \Phi_c)}{\frac{1}{2}(\ell_{ad} + \ell_t) v_{ad}} (X_{ad} - X_t), \end{aligned} \quad (A16)$$

$$\begin{aligned} \frac{\partial T_{ad}}{\partial t} &= \frac{k_{th} A_s}{\frac{1}{2}C \bar{C}_{p,ad}^\ell v_{ad}} \left[\frac{(T_{body} - T_{ad})}{\ell_{ad}} - \frac{\Phi_c (T_{ad} - T_c)}{\ell_{ad}} \right. \\ &\left. - \frac{(1 - \Phi_c)(T_{ad} - T_t)}{(\ell_{ad} + \ell_t)} \right]. \end{aligned} \quad (A17)$$

Alveolar Compartment

The alveolar gas and pulmonary blood spaces are assumed to be separate, well mixed, and without a diffusion barrier between the spaces. On inspiration, the mole fraction of soluble gas entering the alveolar space, $Y_{A,I}$, is equal to the Y_a leaving the 18th generation. On expiration, the mole fraction of soluble gas leaving the alveolar space, Y_A , is the boundary condition for the 18th generation. The mole fraction of soluble gas leaving the blood compartment is assumed to be in equilibrium with the soluble gas mole fraction in the gas space. Throughout the breathing cycle, the alveolar air is assumed to be fully saturated with water and to have a temperature equal to the mean body core temperature, 37°C. The final form of the equation describing conservation of soluble gas in the alveolar compartment can be written for both inspiration [Eq. (A18)] and expiration [Eq. (A19)]:

$$\frac{dY_A}{dt} = \frac{dV_A/dt}{(\lambda_{b:a}V_p + V_A)} \left[(Y_{A,I} - Y_A) + \frac{\dot{Q}_p \lambda_{b:a}}{dV_A/dt} (Y_v - Y_A) \right], \quad (A18)$$

$$\frac{dY_A}{dt} = \frac{dV_A/dt}{(\lambda_{b:a}V_p + V_A)} \left[\frac{\dot{Q}_p \lambda_{b:a}}{dV_A/dt} (Y_v - Y_A) \right], \quad (A19)$$

where

$$Y_v = \frac{RT}{P_t} \frac{\rho}{MW_w} \frac{X_v}{\lambda_{b:a}}.$$

NOMENCLATURE

A	cross-sectional area of the airway lumen (cm ²)
A_s	airway surface area = $\pi d \Delta z$ (cm ²)
C	molar concentration of airway wall (properties of water, assumed) (mol cm ⁻³)
C_a	molar concentration of soluble gas (mol cm ⁻³)
C_g	molar concentration of airway lumen (properties of ideal gas, assumed) (mol cm ⁻³)
$\bar{C}_{p,a}^g$	average volumetric heat capacity of soluble gas in the vapor phase (J mol ⁻¹ °C ⁻¹)
$\bar{C}_{p,da}^g$	average volumetric heat capacity of dry air (J mol ⁻¹ °C ⁻¹)

$\bar{C}_{p,w}^g$	average volumetric heat capacity of water vapor ($\text{J mol}^{-1} \text{ } ^\circ\text{C}^{-1}$)	$k_{y,w}$	local mass transfer coefficient for water ($\text{mol water s}^{-1} \text{ cm}^{-2}$)
$\bar{C}_{p,a}^\ell$	average volumetric heat capacity of soluble gas in the liquid phase ($\text{J mol}^{-1} \text{ } ^\circ\text{C}^{-1}$)	k_{th}	thermal conductivity of tissue ($\text{J cm}^{-1} \text{ s}^{-1} \text{ } ^\circ\text{C}^{-1}$)
$\bar{C}_{p,ad}^\ell$	average volumetric heat capacity of adventitial tissue ($\text{J mol}^{-1} \text{ } ^\circ\text{C}^{-1}$)	ℓ_{ad}	adventitial layer thickness (cm)
$\bar{C}_{p,b}^\ell$	average volumetric heat capacity of blood ($\text{J mol}^{-1} \text{ } ^\circ\text{C}^{-1}$)	ℓ_m	mucous layer thickness (cm)
$\bar{C}_{p,m}^\ell$	average volumetric heat capacity of mucous layer ($\text{J mol}^{-1} \text{ } ^\circ\text{C}^{-1}$)	ℓ_t	connective layer thickness (i.e., distance from the bronchial capillary to the airway lumen) (cm)
$\bar{C}_{p,t}^\ell$	average volumetric heat capacity of connective tissue ($\text{J mol}^{-1} \text{ } ^\circ\text{C}^{-1}$)	$\lambda_{b:a}$	blood:air partition coefficient
$\bar{C}_{p,w}^\ell$	average volumetric heat capacity of water ($\text{J mol}^{-1} \text{ } ^\circ\text{C}^{-1}$)	$\lambda_{b:t}$	blood:tissue partition coefficient
$\Delta \bar{C}_{p,a}^g$	$\bar{C}_{p,a}^g - \bar{C}_{p,da}^g$ ($\text{J mol}^{-1} \text{ } ^\circ\text{C}^{-1}$)	$\lambda_{m:a}$	mucus:air partition coefficient
$\Delta \bar{C}_{p,w}^g$	$\bar{C}_{p,w}^g - \bar{C}_{p,da}^g$ ($\text{J mol}^{-1} \text{ } ^\circ\text{C}^{-1}$)	$\lambda_{t:m}$	tissue:mucus partition coefficient
d	airway diameter (cm)	M_w	molecular weight of water (g mol^{-1})
$D_{a,i}$	molecular diffusion coefficient of gas species, i , through air ($\text{cm}^2 \text{ s}^{-1}$)	n	compartment number
D_L	diffusing capacity of the airway tissue ($\text{cm}^3 \text{ s}^{-1}$)	n_{tot}	total number of moles in the airway lumen (mol)
D_m	molecular diffusion coefficient of soluble gas through mucus ($\text{cm}^2 \text{ s}^{-1}$)	\dot{n}_i	molar evaporation rate of species i from the mucus to airway lumen (mol s^{-1})
D_t	molecular diffusion coefficient of soluble gas through tissue ($\text{cm}^2 \text{ s}^{-1}$)	N	total number of compartments
F	weighting factor that describes the axial dependence of bronchial blood flow (Ref. 5)	P_t	total ambient pressure (mmHg)
FRC	functional residual capacity (cm^3)	\bar{q}_{br}	mean blood flow per unit volume of tissue ($\text{ml blood s}^{-1} \text{ ml tissue}^{-1}$)
Φ_c	capillary area fraction, ratio of surface area participating in exchange between the bronchial capillary and airway	\dot{q}_{br}	airway blood flow within a control volume (ml s^{-1})
g	generation number	\dot{Q}_{br}	total airway blood flow (ml s^{-1})
h	heat transfer coefficient between the mucus and airway lumen ($\text{J s}^{-1} \text{ } ^\circ\text{C}^{-1} \text{ cm}^{-2}$)	\dot{Q}_p	pulmonary blood flow (ml s^{-1})
\bar{H}_a^{vap}	latent heat of vaporization of a soluble gas (J mol^{-1})	R	universal gas constant ($62\,360 \text{ mmHg cm}^3 \text{ mol}^{-1} \text{ K}^{-1}$)
$\bar{H}_{da}^{\text{vap}}$	latent heat of vaporization for dry air (J mol^{-1})	ρ	density of water (g cm^{-3})
\bar{H}_w^{vap}	latent heat of vaporization for water (J mol^{-1})	\dot{S}	total flux of fluid via secretion ($\text{mol s}^{-1} \text{ cm}^{-2}$)
$\Delta \bar{H}_a^{\text{vap}}$	$\bar{H}_a^{\text{vap}} - \bar{H}_{da}^{\text{vap}}$ (J mol^{-1})	t	time (s)
$\Delta \bar{H}_w^{\text{vap}}$	$\bar{H}_w^{\text{vap}} - \bar{H}_{da}^{\text{vap}}$ (J mol^{-1})	T_a	temperature of the airway lumen ($^\circ\text{C}$)
i	number of control volumes in a compartment n	T_{ad}	temperature of the adventitial layer ($^\circ\text{C}$)
I	total number of control volumes	T_{ABS}	absolute temperature of the airway lumen (K)
\dot{j}_{exp}	molar flux of soluble gas into the airway lumen within an airway generation during expiration (mol breath^{-1})	T_b	Body temperature (37°C)
\dot{j}_{insp}	molar flux of soluble gas into the mucous layer within an airway generation during inspiration (mol breath^{-1})	T_c	temperature of blood leaving the bronchial capillary bed ($^\circ\text{C}$)
$k_{y,a}$	local mass transfer coefficient for soluble gas ($\text{mol soluble gas s}^{-1} \text{ cm}^{-2}$)	T_m	temperature of the mucous layer ($^\circ\text{C}$)
$k_{y,i}$	local mass transfer coefficient for species i ($\text{mol } i \text{ s}^{-1} \text{ cm}^{-2}$)	T_t	temperature of the tissue layer ($^\circ\text{C}$)
		TLC	total lung capacity (cm^3)
		v_{ad}	adventitial tissue layer volume (cm^3)
		v_c	bronchial capillary volume (cm^3)
		v_t	volume of tissue surrounding an airway from lumen to alveolar-adventitial boundary of thickness Δz (cm^3)
		VC	vital capacity (cm^3)
		V_{ee}	lung volume at end expiration (cm^3)
		V_{ei}	lung volume at end inspiration (cm^3)
		V_A	alveolar gas volume (cm^3)
		V_p	pulmonary blood volume (cm^3)
		V_t	total volume of airway tissue (cm^3)
		\dot{V}	volumetric flow rate of air ($\text{cm}^3 \text{ s}^{-1}$)
		\dot{V}_A	alveolar ventilation ($\text{cm}^3 \text{ s}^{-1}$)
		\dot{V}_{exp}	volumetric flow rate of air during expiration ($\text{cm}^3 \text{ s}^{-1}$)

\dot{V}_{insp}	volumetric flow rate of air during inspiration ($\text{cm}^3 \text{s}^{-1}$)
X_a	mole fraction of soluble gas in the systemic blood
X_{ad}	mole fraction of soluble gas in the adventitial layer
X_c	mole fraction of soluble gas leaving the bronchial bed
X_m	mole fraction of soluble gas in the mucous layer
X_{pb}	mole fraction of soluble gas in the pulmonary bed layer, $= (X_a + X_v)/2$
X_t	mole fraction of soluble gas in the connective tissue
X_v	mole fraction of soluble gas in the venous blood
Y_a	mole fraction of soluble gas in the airway lumen
Y_A	mole fraction of soluble gas in the alveolar gas space
$Y_{A,i}$	mole fraction of soluble gas entering the alveolar gas space from generation 18
Y_v	mole fraction of soluble gas in air that is in equilibrium with X_v
Y_w	mole fraction of water in the airway lumen
$Y_{\text{wall},a}$	mole fraction of soluble gas at the air–mucus interface
$Y_{\text{wall},w}$	mole fraction of water at the air–mucus interface
z	axial direction (cm)
Δz	control volume length (cm)

REFERENCES

- Agostoni, P., D. J. Godden, and E. M. Balie. Measurement of bronchial blood flow in humans. In: *The Bronchial Circulation*, edited by J. Butler. New York: Marcel Dekker, 1992, pp. 181–196.
- Altman, P. L., and D. S. Dittmer. *Respiration and Circulation*. Bethesda, MD: Federation of American Societies for Experimental Biology, 1971.
- Anderson, J. C., S. L. Bernard, D. L. Luchtel, A. L. Babb, and M. P. Hlastala. Axial and radial distribution of the bronchial vasculature in sheep. *Respir. Physiol. Neurobiol.* 132:329, 2002.
- Baile, E. M., and P. D. Pare. Methods of measuring bronchial blood flow. In: *The Bronchial Circulation*, edited by J. Butler. New York: Marcel Dekker, 1992, pp. 101–180.
- Bernard, S. L., R. W. Glenny, N. L. Polissar, D. L. Luchtel, and S. Lakshminarayan. Distribution of pulmonary and bronchial blood supply to airways measured by fluorescent microspheres. *J. Appl. Physiol.* 80:430–436, 1996.
- Bui, T. D., D. Dabdub, and S. C. George. Modeling bronchial circulation with application to soluble gas exchange: Description and sensitivity analysis. *J. Appl. Physiol.* 84:2070–2088, 1998.
- Chilton, T. H., and A. P. Colburn. Mass transfer (absorption) coefficients: Prediction from data on heat transfer and fluid friction. *Ind. Eng. Chem.* 26:1183–1187, 1934.
- Deffebach, M. E., N. B. Charan, S. Lakshminarayan, and J. Butler. The bronchial circulation. Small, but a vital attribute of the lung. *Am. Rev. Respir. Dis.* 135:463–481, 1987.
- Eger, E. I., and C. P. Larson, Jr. Anaesthetic solubility in blood and tissues: Values and significance. *Br. J. Anaesth.* 36:140–149, 1964.
- Farhi, L. E. Elimination of inert gas by the lung. *Respir. Physiol.* 3:1–11, 1967.
- Gastineau, R. M., P. J. Walsh, and N. Underwood. Thickness of bronchial epithelium with relation to exposure to radon. *Health Phys.* 23:857–860, 1972.
- George, S. C., A. L. Babb, M. E. Deffebach, and M. P. Hlastala. Diffusion of nonelectrolytes in the canine trachea: Effect of tight junction. *J. Appl. Physiol.* 80:1687–1695, 1996.
- George, S. C., A. L. Babb, and M. P. Hlastala. Dynamics of soluble gas exchange in the airways. III. Single-exhalation breathing maneuver. *J. Appl. Physiol.* 75:2439–2449, 1993.
- George, S. C., J. E. Souders, A. L. Babb, and M. P. Hlastala. Modeling steady-state inert gas exchange in the canine trachea. *J. Appl. Physiol.* 79:929–940, 1995.
- Gerde, P., and B. R. Scott. A model for absorption of low-volatile toxicants by the airway mucosa. *Inhalation Toxicol.* 13:903–929, 2001.
- Hanna, L. M., and P. W. Scherer. Regional control of local airway heat and water vapor losses. *J. Appl. Physiol.* 61:624–632, 1986.
- Hildebrandt, J. Structural and mechanical aspects of respiration. In: *Textbook of Physiology*, edited by H. D. Patton, A. F. Fuchs, B. Hille, A. M. Scher, and R. Steiner. Philadelphia: W. B. Saunders, 1989, pp. 991–1011.
- Hindmarsh, A. LSODE (Computer Software). Livermore, CA: Lawrence Livermore Laboratory, 1981.
- Hlastala, M. P. The alcohol breath test: A review. *J. Appl. Physiol.* 84:401–408, 1998.
- Hlastala, M. P., and A. J. Berger. *Physiology of Respiration*. New York: Oxford University Press, 1996.
- Hu, S. C., A. Ben-Jebria, and J. S. Ultman. Simulation of ozone uptake distribution in the human airways by orthogonal collocation on finite elements. *Comput. Biomed. Res.* 25:264–278, 1992.
- Ingenito, E. P. *Respiratory Fluid Mechanics and Heat Transfer* (Ph.D.). Cambridge, MA: Massachusetts Institute of Technology, 1984.
- Johanson, G., and B. Dynesius. Liquid air partition coefficients of 6 commonly used glycol ethers. *Br. J. Ind. Med.* 45:561–564, 1988.
- Jones, A. W. Determination of liquid air partition-coefficients for dilute solutions of ethanol in water, whole-blood, and plasma. *J. Anal. Toxicol.* 7:193–197, 1983.
- Jones, A. W. Quantitative measurements of the alcohol concentration and the temperature of breath during a prolonged exhalation. *Acta Physiol. Scand.* 114:407–412, 1982.
- Jones, A. W., S. Skagerberg, T. Yonekura, and A. Sato. Metabolic interaction between endogenous methanol and exogenous ethanol studied in human volunteers by analysis of breath. *Pharmacol. Toxicol.* 66:62–65, 1990.
- Kaneko, T., P. Y. Wang, and A. Sato. Partition-coefficients of some acetate esters and alcohols in water, blood, olive oil, and rat-tissues. *Occup. Environ. Med.* 51:68–72, 1994.
- Kumagai, S., and I. Matsunaga. A lung model describing uptake of organic solvents and roles of mucosal blood flow and metabolism in the bronchioles. *Inhalation Toxicol.* 12:491–510, 2000.
- Kumagai, S., H. Oda, I. Matsunaga, H. Kosaka, and S. Akasaka. Uptake of 10 polar organic solvents during short-term respiration. *Toxicol. Sci.* 48:255–263, 1999.
- Kuwano, K., C. H. Bosken, P. D. Pare, T. R. Bai, B. R. Wiggs, and J. C. Hogg. Small airways dimensions in asthma

- and in chronic obstructive pulmonary disease. *Am. Rev. Respir. Dis.* 148:1220–1225, 1993.
- ³¹ Lopez-Vidriero, M. T., I. Das, and L. M. Reid. Airway secretion: Source, Biochemical and Rheological Properties. In: *Respiratory Defense Mechanisms*, edited by J. D. Brain, D. F. Proctor, and L. M. Reid. New York: Marcel Dekker, 1977, pp. 289–356.
- ³² Lowe, H., and K. Hagler. Determination of volatile organic anaesthetics in blood, gases, tissues and lipids: Partition Coefficients. In: *Gas Chromatography in Biology and Medicine*, edited by R. Porter. London: Churchill, 1969, pp. 86–103.
- ³³ Onorato, D. J., M. C. Demirozu, A. Breitenbucher, N. D. Atkins, A. D. Chediak, and A. Wanner. Airway mucosal blood flow in humans. Response to adrenergic agonists. *Am. J. Respir. Crit. Care Med.* 149:1132–1137, 1994.
- ³⁴ Sato, A., and T. Nakajima. Partition-coefficients of some aromatic-hydrocarbons and ketones in water, blood and oil. *Br. J. Ind. Med.* 36:231–234, 1979.
- ³⁵ Schrikker, A. C., W. R. de Vries, A. Zwart, and S. C. Luijendijk. The excretion of highly soluble gases by the lung in man. *Pfluegers Arch.* 415:214–219, 1989.
- ³⁶ Schrikker, A. C., W. R. de Vries, A. Zwart, and S. C. Luijendijk. Uptake of highly soluble gases in the epithelium of the conducting airways. *Pfluegers Arch.* 405:389–394, 1985.
- ³⁷ Schwardt, J. D., S. R. Gobran, G. R. Neufeld, S. J. Aukburg, and P. W. Scherer. Sensitivity of CO₂ washout to changes in acinar structure in a single-path model of lung airways. *Ann. Biomed. Eng.* 19:679–697, 1991.
- ³⁸ Solway, J., A. R. Leff, I. Dreshaj, N. M. Munoz, E. P. Ingenito, D. Michaels, R. H. Ingram, and J. M. Drazen. Circulatory heat-sources for canine respiratory heat exchange. *J. Clin. Invest.* 78:1015–1019, 1986.
- ³⁹ Souders, J. E., S. C. George, N. L. Polissar, E. R. Swenson, and M. P. Hlastala. Tracheal gas exchange: Perfusion-related differences in inert gas elimination. *J. Appl. Physiol.* 79:918–928, 1995.
- ⁴⁰ Swenson, E. R., H. T. Robertson, N. L. Polissar, M. E. Middaugh, and M. P. Hlastala. Conducting airway gas exchange: Diffusion-related differences in inert gas elimination. *J. Appl. Physiol.* 72:1581–1588, 1992.
- ⁴¹ Treybal, R. E. *Mass Transfer Operations*. New York: McGraw-Hill, 1980.
- ⁴² Tsu, M. E., A. L. Babb, D. D. Ralph, and M. P. Hlastala. Dynamics of heat, water, and soluble gas exchange in the human airways: 1. A model study. *Ann. Biomed. Eng.* 16:547–571, 1988.
- ⁴³ Tsu, M. E., A. L. Babb, E. M. Sugiyama, and M. P. Hlastala. Dynamics of soluble gas exchange in the airways: II. Effects of breathing conditions. *Respir. Physiol.* 83:261–276, 1991.
- ⁴⁴ Twedt, M. M. *An Analysis of the Effects of Axial Dispersion and Tissue Solubility on Gas Exchange in the Upper Airways* (M.S.). Seattle, WA: University of Washington, 1996.
- ⁴⁵ Wagner, P. D., P. F. Naumann, and R. B. Laravuso. Simultaneous measurement of eight foreign gases in blood by gas chromatography. *J. Appl. Physiol.* 36:600–605, 1974.
- ⁴⁶ Wagner, P. D., H. A. Saltzman, and J. B. West. Measurement of continuous distributions of ventilation-perfusion ratios: Theory. *J. Appl. Physiol.* 36:588–599, 1974.
- ⁴⁷ Weibel, E. R. *Morphometry of the Human Lung*. New York: Academic, 1963.
- ⁴⁸ Widmark, E. M. P. *Principles and Applications of Medicolegal Alcohol Determination* (Die theoretischen Grundlagen und die Praktische Verwendbarkeit der gerichtlichmedizinischen Alkoholbestimmung, Berlin:1932). Davis, CA: Biomedical, 1981.
- ⁴⁹ Wilhelm, E., R. Batting, and R. Wilcock. Low-Pressure Solubility of Gases in Liquid Water. *Chem. Rev. (Washington, D.C.)* 77:219, 1977.
- ⁵⁰ Wilke, C. R., and P. Chang. Correlation of diffusion coefficients in dilute solutions. *AIChE J.* 1:264–270, 1955.
- ⁵¹ Yaws, C. L., J. R. Hopper, S. D. Sheth, M. Han, and R. W. Pike. Solubility and Henry's law constant for alcohols in water. *Waste Manage.* 17:541–547, 1997.
- ⁵² Yaws, C. L., S. D. Sheth, and M. Han. Using solubility and Henry's law constant data for ketones in water. *Pollution Eng.* 22:70–75, 1998.
- ⁵³ Young, I. H., and P. D. Wagner. Solubility of inert gases in homogenates of canine lung tissue. *J. Appl. Physiol.* 46:1207–1210, 1979.